Flexible Ultralow Power Sensor Interfaces for E-Skin

Chen Jiang, *Member, IEEE*, Xiang Cheng, *Member, IEEE*, and Arokia Nathan, *Fellow, IEEE*

***Abstract*—Thin-film electronics has hugely benefitted from low-cost processes, large-area processability, and multi-functionality. This has not only stimulated innovation in display and sensor technology, but has also demonstrated great potential for integration of components for human-machine interfaces. For electronics to be deployed as sensor interfaces and signal processing, the quest for low power is compelling due to the inherently limited battery lifetime. This review will present the state-of-the-art in thin film electronics and demonstrate examples of low-cost printable transistors and biosensors that are flexible/stretchable for wearable and other applications. Ultralow power design for thin-film transistors will be discussed from the standpoint of reducing both operating voltage and operating current, taking into account the challenges in meeting frequency requirements. Compact models for circuit design will be reviewed along with new insights into ultralow power transistors and high gain amplifier circuits. Finally, a concept for an integrated system comprising sensors and interfacing circuits will be demonstrated, which has the potential to enable battery-less operation.**

***Index Terms*—flexible electronics, human-computer interaction, low-power electronics, thin film transistors.**

I. Introduction

ELECTRONIC skin (e-skin) has enabled devices that can mimic the functionalities of human skin and/or monitor humans in real time for continuous healthcare management [1]–[3]. Therefore, e-skin is an indispensable component for humanoids and human-computer interactions. Despite considerable developments and demonstrations of multi-sensing skin [4] and self-powered e-skin [5], several fundamental requirements still need to be fulfilled to maximize the potential of this technology. The most striking requirements include increasing the comfort of electronics to be worn on the skin and the ability to acquire as much human physiological information as possible [6], [7]. In addition, e-skin relies on batteries and warrants eco-friendly electronic devices, so minimizing power consumption and fabrication costs are important [7]–[11]. Although there have been considerable studies in low power design in conventional silicon technology [12]–[16], the leakage (and hence, operating) currents are higher as compared to wider band-gap materials such as the semiconducting oxide [17]–[19] or thieno[3,2-b]thiophene-based organic semiconductor [20]–[22] families. However, the realization of low-power signal conditioning and transmission circuits using these materials families remain a challenge and is wide open to further investigation.

An empowering alternative to conventional silicon, including thinned-down silicon, technology for e-skin is thin-film electronics, which can be manufactured by direct additive processes (e.g., inkjet printing), produced to form relatively thin (nm-scale) structures, and amenable to large area (m^2) scaling [17], [23]–[30], as conceptualized in Fig. 1 for a sensor interface system for e-skin. Since e-skin applications are more varied and require smaller production runs than is typical of silicon technologies, thin-film device fabrication has considerable cost benefits, in particular, with printing-based processes [11], [31], [32]. Form factor and potential bendability are other key characteristics, and an appropriate choice of materials and device structures is necessary to maintain mechanical robustness [6], [21], [33], [34]. Here, device and circuit modeling are indispensable for the design of low-power,

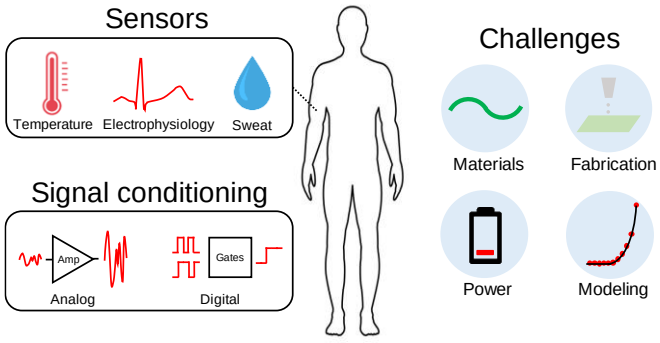

Fig. 1. A conceptualized thin film electronics based sensor interface system for e-skin and its requirements. A variety of TFT-based sensors are used to acquire human physiological information. Analog and digital circuits are built-in for signal conditioning. E-skin requires materials used to be flexible, low-cost fabrication, low power consumption, and a good model for TFT circuit design.

This work was supported in part by EPSRC under Project EP/M013650/1, and EU under Projects DOMINO 645760, 1D-NEON 685758 and BET-EU 692373, IEEE Electron Devices Society PhD Student Fellowship, and China Scholarship Council.

The authors were from the Department of Engineering, University of Cambridge, Cambridge CB3 0FA, UK, where the work was carried out.

C. Jiang is now with Department of Clinical Neurosciences, University of Cambridge, Cambridge Biomedical Campus, CB2 0QQ, UK (e-mail: cj360@cam.ac.uk).

X. Cheng and **A. Nathan** are now with Cambridge Touch Technologies Ltd, Cambridge CB4 0GN, UK (e-mail: anathan@camtouch3d.com).

Table 1. Basic performance and fabrication specifications comparison for TFT technologies.

TFT technologies	a-Si	LTPS	IGZO	Organics
Material				
Band-gap (eV)	~1.8	~1.1	>3	1~3
Density of deep states (cm^{-3} eV^{-1})	~10^{18}	~10^{18}	~10^{17}	>10^{14}
Flexibility	No	No	Limited	Good
Printability	Limited	Limited	Limited	Good
Device				
***SS* (V/dec) (*SS* variation)**	0.5 (~0.2)	0.2~1 (~0.1)	0.1~0.3 (~0.02)	0.05~1 (0.01~0.2)
V_T (V) (V_T variation)	~5 (~0.5)	~5 (~1)	>1 (~0.2)	~0 (~0.1)
I_{ON}/I_{OFF}	~10^7	~10^7	>10^7	>10^6
Operating voltage (V)	2~20	2~20	2~5	1~10
Circuit				
Amplifier gain (V/V)	10~50	20~100	10~200	5~260
Power consumption (W)	>100n	~1μ	1n~1μ	1n~1μ
Fabrication				
Process temperature (°C)	~350	~500	>200	<130
Equipment cost ($)	>1 million	>1 million	~1 million	~40,000
Layout cost ($/$m^2$)	~400,000	~800,000	~500,000	~0
Material waste	>80%	>80%	30~80%	<1%

strain-immune circuits. This will benefit device/battery operational lifetime as well as sensitivity to physiological signals (which are typically voltage signals of less than 1 millivolt) [35]–[38]. With these potential benefits, thin-film electronics is likely to enable new possibilities for e-skin, specifically addressing low cost, low power, mechanical flexibility, and high signal sensitivity.

To construct a sensor interface, a variety of thin-film sensors are required to acquire human physiological information, and analog and digital circuits need to be co-integrated for signal conditioning and transmission (Fig. 1). There have been considerable papers reporting on-skin sensor interfaces [39], including thin-film sensors [40], [41], amplifier [6], [42], and wireless power transfer blocks [43], [44]. Most of these systems, however, are not solely thin-film electronics based, which could result in bulky devices that need to be worn on skin [45].

In Section II of this review, we present printable and flexible materials for thin-film electronics, and in particular, thin-film transistors (TFTs), which constitute a fundamental building block. We discuss different materials for TFTs and mainly focus on the manufacturing processability and the key features of TFTs. Then, we introduce and compare different printing technologies for low-cost printed electronics. Section III reviews the current development of printed TFTs. In addition, examples of low-cost printable transistor-based biosensors that are flexible/stretchable are reviewed, including pressure mapping, heartbeat monitoring, temperature capturing, electrophysiology recording, and ion detection. Section IV discusses design issues related to ultralow power TFT operation for e-skin, including reducing the operating voltage and operating current of TFTs. In addition, Schottky-barrier subthreshold TFTs are discussed, with the merits of ultralow power, high intrinsic gain for signal amplification, and geometry-independent characteristics that accommodate the large geometrical variation of printed TFTs. Other specifications for sensor interfaces are discussed, including cut-off frequency and noise. Compact models for TFT circuit designs are reviewed in Section V, along with the density of states (DOS) extraction, DC signal modeling, and small signal modeling. Finally, a concept for an integrated system comprising sensors and interfacing circuits is demonstrated, which has the potential to enable battery-less operation.

II. Printing Technologies for Thin-Film Electronics

A. Printable and Flexible Materials

For sensor interfaces in e-skin, the most fundamental and essential component is the thin-film transistor (TFT). Typical TFT technologies are based on four types of materials and structures, including amorphous silicon (a-Si) [46], [47], polycrystalline silicon (poly-Si) [48]–[51], amorphous oxide semiconductors (AOS) [52]–[65], and organics [21], [27], [34], [66]. Compared to organics, the former three have limited printability and flexibility (Table 1). Though there are some reports on printable silicon and AOS, they required high process temperatures (generally >200 °C) and their device performance was not as good as vacuum processed ones [67]–[76]. For TFTs to be deployed on skin, their substrates require mechanic flexibility. Good substrate candidates are polymers, such as polyethylene terephthalate (PET), polyethylene naphthalate (PEN), and polyimide (PI), but their glass transition temperatures are < 200 °C. Therefore, the process temperatures for silicon-based TFTs are still too high, and low-temperature (i.e., < 200 °C) processable semiconductor alternatives are demanded. Apart from these materials, there are also some other types of materials that have demonstrated high device performance, such as carbon nanotubes [77]–[80],

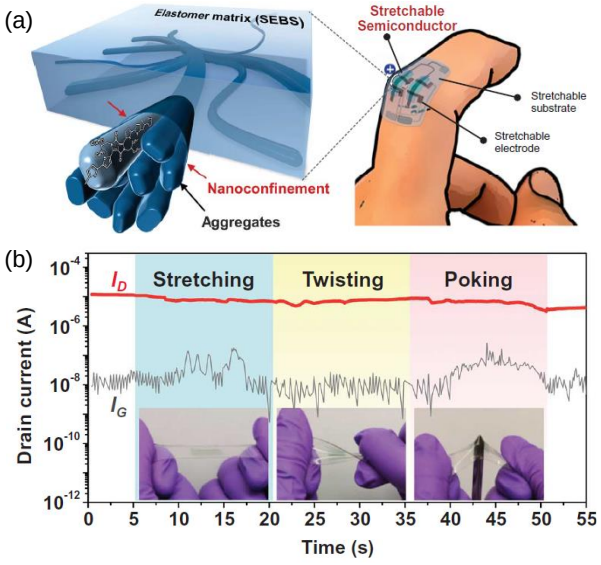

Fig. 2. Nanoconfinement effect for enhancing the stretchability of polymer semiconducting film and organic TFT. (a) A 3D schematic of the desired morphology composed of embedded nanoscale networks of polymer semiconductor to achieve high stretchability, which can be used to construct a highly stretchable and wearable TFT. (b) Drain current (I_D) and gate current (I_G) of a fully stretchable TFT under sequential stretching, twisting, and poking with a sharp object. Adapted from [34].

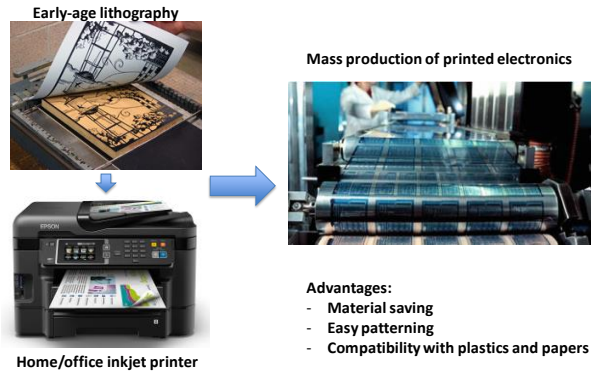

Fig. 3. From printing documents to printing electronics.

nanowires [81], [82], transfer printed silicon [68], [69], molybdenum disulphide and other 2-dimensional materials [83]–[86]. With recent development of organics, organic TFTs have demonstrated comparable performance to the vacuum processed TFTs. In this section, we will focus on organics that are printable and flexible, which are essential for e-skin.

Organic semiconductor materials are carbon-based compounds that consist of π-conjugation systems, which contribute to electron/hole charge transport. Depending on their molecular structures, organic semiconductor materials can be categorized into small molecules and polymers depending on their molecular structures. The most common small molecules include rubrene [87], pentacene (and its derivatives) [88], anthradithiophene (ADT) derivatives [89], and benzothieno[3,2-b] [1], benzothiophene (BTBT) derivatives [90]. Most polymer semiconductors are thiophene-based, such as region-regular poly (3-hexylthiophene-2,5-diyl) (P3HT) [91] and indacenodithiophene-co-benzothiadiazole (IDT-BT) [92]. In general, small molecules can form well-ordered crystalline phases and thus demonstrate higher mobilities; however, mobilities of small molecules depend on the stacking directions of molecules [93], which are randomly distributed by most deposition methods (e.g., spin-coating, inkjet printing), resulting in a large variation of mobility values. In contrast, polymers are normally in amorphous phases, which yield better uniformities but lower mobilities (< 1 $cm^2V^{-1}s^{-1}$). The first organic TFT was invented by Koezuka et al. using polymer semiconductor, polythiophene in 1987, but the mobility was only 2×10^{-5} $cm^2V^{-1}s^{-1}$ [94]. In the past three decades, significant developments in organic semiconductors have been achieved, with a high mobility of >10 $cm^2V^{-1}s^{-1}$ in both small molecules and polymers [95].

The most striking advantage of organics is their solution processability. Although silicon and AOS are also solution-processible, they need high process temperatures for precursors to react and form the desired materials and structures. In contrast, organics can easily dissolve in compatible organic liquids, which simplifies the processes of ink formulation and post-deposition reactions/treatments. This feature of organics enables organic TFTs and circuits printable on plastics with process temperatures of lower than 130 °C [96]. In addition, all-printed organic TFTs have been reported [11], [97], [98]. However, conventional solution-processed organic TFTs require high operating voltages of several tens of volt, which contradicts the idea of low power. To tackle this issue, considerable effort has been made to lower the operating voltage of organic TFTs, and reports have demonstrated low an operating voltage of less 1 V, which has greatly reduced the power consumption for TFT operation [99]–[101]. Further discussion on power consumption in TFT can be found in Section IV.

Another advantage of organics is their mechanic flexibility. In contrast to silicon and metal oxides that are covalently bonded, organic molecules are van der Waals bonded and therefore can restore themselves from certain bending deformations. Someya and his coworkers have developed organic TFTs with both n-type and p-type devices and integrated them into circuits, demonstrating extreme bending stability [33], [102]. The same research group has reported ultra-flexible and ultra-lightweight organic TFTs, which are potential candidates for imperceptible electronics to be employed on the skin [21]. In recent years, intrinsically stretchable organic semiconducting materials have been achieved by Bao and her coworkers through the nanoconfinement of polymers into nanometer-scale dimensions (see Fig. 2), which can alter many polymer physical properties, including lowering the mechanical modulus and glass transition temperature and increasing the mechanical ductility [6], [34]. In addition to flexibility and stretchability, organic TFTs have also been developed as essential components for sensors [103], radio frequency identification (RFID) tags [104], smart memories [105], point-of-care diagnostic systems [106] and wearable systems [107]. With good compatibility to the skin, the organic TFT-based e-skin has been developed [2].

In addition to conventional organic TFT structures, there is another family of organic transistors, organic electrochemical transistors (OECTs), that can be used for chemical/biological sensing [108] and mimicking synapses [109]. Malliaras et al. used OECTs demonstrated *in vivo* brain activity recording [29]. They found that different from conventional transistors, OECTs have volumetric capacitance characteristics and therefore demonstrate low operating voltages and high transconductance [110]–[112].

Due to these features of organics, in the following discussions on sensor interfaces, we will focus on printable and flexible organic TFTs.

B. Printing Techniques

Patterning electronic materials is important to achieve integrated films and patterns that can function as an electronic device [113]. For conventional fabrication of electronic devices, i.e., silicon MOSFETs, the wastage of materials is huge, since all the material deposition processes involve photolithography and need to be subtracted. Compared to photolithography, printing is more straightforward, and the patterning of materials can be achieved by so-called direct patterning, i.e., depositing materials only on the wanted areas. In this way, material wastage can be greatly reduced. Therefore, printing techniques are suitable to meet the low-cost requirements of e-skin fabrication, where low fabrication cost and negligible material waste are important criteria. Regarding TFT technologies, here we focus on printable organic TFTs,

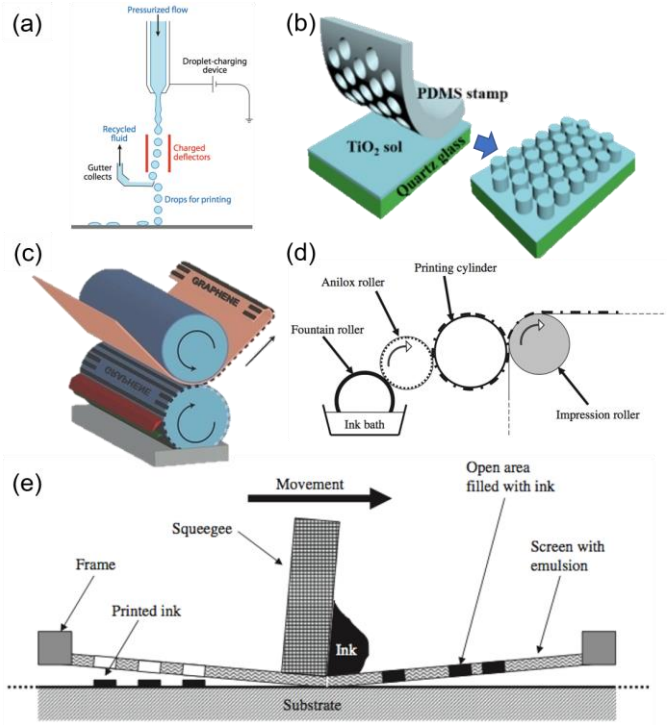

Fig. 4. Schematics of different printing techniques: (a) inkjet printing, adapted from [114]; (b) nano-imprinting, adapted from [117]; (c) gravure printing, adapted from [120]; (d) flexographic printing, adapted from [113]; (e) screen printing, adapted from [113].

which have better compatibility with printing technologies and better mechanical flexibility as previously mentioned.

1) Inkjet Printing

Inkjet printing is the most promising printing technique which can produce high-resolution 2-dimensional patterns. An inkjet printer consists of a cartridge and a printhead [114]. The cartridge contains ink and supplies the ink to the printhead. The printhead is a sophisticated micro-scale system, which pumps the ink through nozzles to form jetted droplets, as shown in Fig. 4(a). The printhead is designed to be resistant to organic solvents, which allows a wide range of solvents for ink formulation, and therefore the inkjet printing technique is compatible with various printable materials. Inkjet printing has several advantages, including good resolution, little material waste, the potential for customization, and no contact between the printhead and substrate [115].

2) Imprint and Nano-imprint

Imprint achieves patterning by physically deforming a deposited thin-film resist material through a micro/nano-structured mold [116], [117]. The resist material can be thermal or UV-curable [118]. For example, as shown in Fig. 4(b), a UV curable material is deposited on a quartz substrate and then deformed by the mold. After UV exposure, the deformed layer is fixed with a pattern formed by the mold. Though the process is simple, it can produce patterns with good definition and high resolution, which are determined by the mold. The disadvantages of imprinting are air bubbles and ink sticking [118]. When the mold imprints the resist film, some areas make contact at the end, which can induce some air bubbles within these areas. The de-molding process may also cause damage to the patterned layer, since the material though cured can still stick to the mold.

3) Gravure Printing

The gravure printing technique is increasingly complex as it offers high-speed, roll-to-roll deposition of functional materials at high resolution [119]. The process consists of a 2-roller system, where the printing roller has engraved patterns [120], as shown in Fig. 4(c). The printing roller is partly immersed in the ink bath, so that the ink can be continuously refilled. The excess ink is doctored off the printing roller to prevent accumulation in undesired areas. Since the printing roller makes strong enough contact with the rubber supporting roller, the ink in the gravure is transferred from the substrate to form patterns. The disadvantage of gravure printing is that it requires a new costly engraved roller to change new patterns. The advantage is that the web speed can be 1-10 m/s which meets the requirement of the roll-to-roll process [114]. Gravure printing has been used in printing organic and inorganic photovoltaics [121], [122], and it has potential in conductive inks, RFID tags, logic and memory circuits [113].

4) Flexographic printing

Flexographic printing is similar to gravure printing, except that the ink is on the convex area of the printing cylinder/roller rather than in the concave area. In this case, in order to avoid excess ink, an anilox roller is used to refill a measured amount of ink into the printing cylinder, as shown in Fig. 4(d). Therefore, a typical flexographic printing system is a four-roller system, containing a fountain roller, an anilox roller, a printing cylinder, and an impression roller. The process is simple, and the only requirement is less volatile inks. Flexographic printing has potential in smart packaging [123], transparent conductive films [124], logic circuits [125], etc.

5) Screen Printing

Screen printing consists of a screen of woven material and a squeegee, as shown in Fig. 4(e). The pattern of the screen is obtained by partially filling the screen with an emulsion which prevents ink from contacting the substrate. Screen printing is currently widely used in industry for simple patterns such as printing etch resists and conductors for flexible electronics [113]. It can also be fully adapted to a roll-to-roll process with a rotary screen.

6) Comparison of different printing techniques

Due to different printing principles, these printing techniques can result in various qualities and features of printed patterns. Table 2 shows a comparison of the features of the printing methods. Among these printing techniques, imprint yields the highest resolution of <1 μm, which is attributed to the high-resolution mold used in imprinting. Flexographic and gravure printing techniques can provide similar feature sizes of several tens of microns and have similar requirements for ink viscosity. Screen printing requires very high viscosity of inks (>500 mN m^{-1}), and screen printed features are very thick, i.e., >5 μm, which is not appropriate for printed dielectrics whose

Table 2. Comparison of different printing techniques.

Printing technique	Resolution (μm)	Thickness (μm)	Ink viscosity (cPs)	Mismatch (μm)
Inkjet	~20	0.01~0.5	5~30	~20
Nano-imprint	<1	~0.1	-	<1
Gravure	~20	0.5~10	100~1000	~20
Flexographic	~15	0.5~1	50~500	~30
Screen	~50	>2	>500	~40

thickness is around 100 nm. As for inkjet printing, it can produce a similar resolution to most printing techniques (except imprint), and it does not require inks to be highly viscous.

For printed flexible electronics, matching accuracy is important to the realization of circuit and system level applications. Inkjet printing generally induces ~20 μm mismatch [126], due to the flight of droplets. The mismatch of screen printing can be up to 40 μm due to the movement of the screen by squeegee [127]. The mismatch of gravure and flexographic printing depends on the number of rolls and is around 20~30 μm [128]. Nano-imprint only induces <1 μm mismatch, due to the high resolution of lithography [129].

Overall speaking, inkjet printing is a good choice as a printing technique for TFT fabrication. In addition, inkjet printing has the crucial advantage that its customization capacity is high. The research and development of organic TFTs in laboratories or start-ups use trial and empirical patterns of devices, so it is important that the printing technique provides flexibility in pattern designs. This flexibility enabled by inkjet printing can save a considerable amount of time and money, compared to other thin film deposition techniques which need masks, molds, or gravures.

III. Printable and Flexible Transistors

A. TFT Device Architectures

In general, there are four possible TFT device architectures, including bottom-gate bottom-contact (coplanar), bottom-gate top-contact (staggered), top-gate bottom-contact (inverted staggered), and top-gate top-contact (inverted coplanar) structures, as seen in Fig. 5.

For ultralow power e-skin, the operating voltages of organic TFTs should be low, which can be achieved by reducing defects/traps in TFTs. Details on lowering operating voltages are explained in Section IV.A. In brief, for low-voltage TFTs, the semiconductors should be crystallized, and the semiconductor/dielectric interfaces should be smooth. These factors need to be taken into consideration when selecting TFT device architectures. For organic semiconductors, small molecules are much more likely to crystallize compared to polymer semiconducting materials, but they tend to generate a rough surface. For dielectrics, polymers normally demonstrate smooth surfaces, which can be used as a base for the semiconductor/dielectric interface to reduce the interface trap density. In addition, small molecule semiconductors are more vulnerable to heat with regard to the reorganization of crystals and even evaporation. The source/drain electrodes (which need high-temperature annealing) should be deposited prior to the deposition of the semiconductor. Therefore, to achieve printable low-voltage organic TFTs, the bottom-gate bottom-contact structure is preferred, while regarding materials, small-molecule semiconductors and polymer gate insulators are preferred.

Despite of low-voltage consideration, other device architectures have other advantages. Staggered and inverted staggered architectures can greatly reduce the contact resistance between the semiconductor and source/drain electrodes [130]. In these two architectures, charge carriers not only injected from the edge of the source electrode, but also from the area of the electrode that is overlapped with the gate

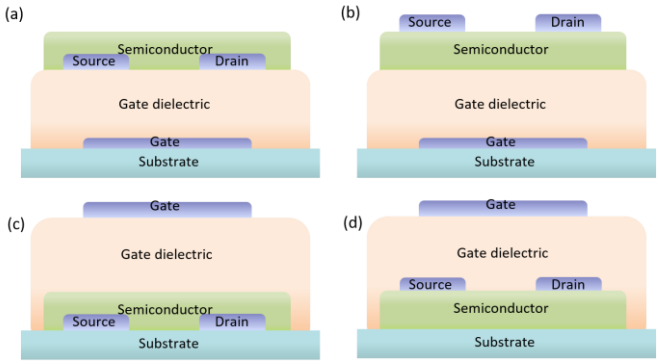

Fig. 5. Schematic diagram of the four TFT device architectures: (a) bottom-gate bottom-contact, (b) bottom-gate top-contact, (c) top-gate bottom-contact, and (d) top- gate top-contact.

electrode. Top gate architectures allow self-aligned TFTs, which use source/drain patterns to define gate pattern [131] or vice versa [132]. In self-aligned TFTs, the overlap between the source/drain electrodes and gate electrode is small, and therefore, parasitic capacitance is reduced. Noh et al. demonstrated self-aligned all-printed polymer TFTs with parasitic overlap capacitance to values as low as 0.2~0.6 pF/mm, and cut-off frequencies of f_T = 1.6 MHz [131].

For e-skin, the variation of TFT performance due to the bending/stretching of substrates is a major issue. As discussed in Section II A, there are a considerable number of reports on flexible and stretchable organic TFTs [6], [21], [33], [34], [102]. Though these works have a great breakthrough in achieving functional devices during bending/stretching, the device performance varies. There are several ways to mitigate the strain, such as wavy [133], mesh [134], and serpentine designs [135]. In addition to these horizontal compensation methods, Sekitani et al. developed a vertical TFT structure to minimize the strain during bending and demonstrated ultra-flexible TFTs without appreciable performance change under <0.1mm bending radius [33]. Such good flexibility and bending stability very was enabled by a thin plastic substrate (12.5μm) and an encapsulation layer of the same thickness that place the transistors in the neutral strain position. It is noteworthy that the device performance also varies even when the same strain is along and perpendicular to the channel length direction [33], [136], which is important for the design of flexible devices/circuits that how the strain to the different directions can be compensated.

B. Issues of Printed Organic TFTs

The main issues in organic TFTs (either vacuum- or solution-processed) are the high operating voltage and poor stability, specifically short shelf-life time and significant threshold voltage shift under bias stress.

The most straightforward way to lower the operating voltage is to increase unit-area gate capacitance [21], [137]. However, this method induces large gate leakage or interface dipole disorder [138], thus exacerbating instability. An alternative way is reducing semiconductor/dielectric interface traps, which in turn can also enhance device stability [139]. However, printed thin films are not as good as vacuum-processed thin films, with regard to the defects and surface roughness of the films. These can significantly generate a considerable number of traps and are the key challenges that need to be tackled.

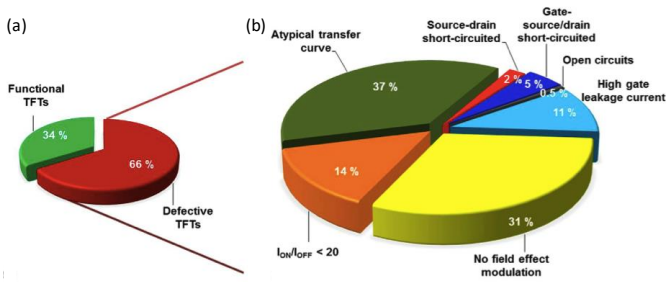

Fig. 6. The proportion of functional TFTs to defective TFTs, adapted from [97].

Instability prevails in most organic TFTs, either vacuum-processed or solution-processed. The instability of organic TFTs can be attributed to intrinsic (e.g., structural and energetic disorder in the semiconductor) and extrinsic factors (e.g., oxidation, presence of moisture, and chemical impurities) [140], [141]. These can induce degradation of device performance during storage in the ambient environment and a threshold voltage shift of the organic TFTs under electrical bias stress [142]. During bias stress, trapped charges can be created in the dielectric (which holds the high electric field) and at the semiconductor/dielectric interface (where charge carriers transport). In order to achieve highly stable all-printed organic TFTs, it is important that:

- there are few defects in the organic TFTs, in particular, in the bulk semiconductor, in the dielectric and at the semiconductor-dielectric interface;
- organic TFTs are encapsulated to avoid material oxidation;
- materials used are water-proof but organic-solvent-like, which avoid moisture while making printing possible.

Besides challenges in organic TFTs, printed devices have other particular issues associated with the inkjet printing technique. One study has reported statistical analysis of the printed organic TFTs, depicting a low proportion of functional devices (34%) as compared to defective devices (Fig. 6) [97]. The reasons for the failures can be categorized into wetting, satellite drops, droplet jetting oddness, dirt and dust particles, as well as missing droplets [143]. Therefore, in order to improve the yield and device performance of all-inkjet-printed organic TFTs, it is essential to ensure that:

- the jetting properties of inks are in good condition, e.g., without satellites;
- the materials used have adequate compatibility, with regard to wetting;
- the quantities of dirt and dust are as small as possible.

C. Current Development of Printable Organic TFTs

1) Methods of Organic Semiconductor Deposition

In previous work on solution-processed/printable organic TFTs, most interest has centered on semiconductor materials. In the early years (the 2000s), most works used silicon wafers as the substrate, utilizing highly doped silicon as the conductive gate and thermally grown SiO_2 as the gate dielectric layer [144]–[146]. However, due to the poor interface between SiO_2 and the organic semiconductor materials, self-assembled monolayers (SAMs) were grown on the SiO_2 to facilitate charge transport at the semiconductor/dielectric interface [147], such as octadecyl-, decyl-, and butyltrichlorosilane (OTS, DTS, and BTS). At that time, typical solution-processable organic semiconductor materials were P3HT (polymer) [10], [140] and TIPS-pentacene (small molecule) [88], [148], and the mobility of the fabricated organic TFTs was low, generally less than 0.1 $cm^2V^{-1}s^{-1}$. However, polymer semiconductor materials are amorphous, and it is not easy to control their crystallization.

In the past decade, significant effort has been made to grow highly crystallized organic semiconductor materials, using drop casting [139], [149] and blade coating [147], [150], [151]. Optical polarized photos of TIPS-pentacene thin films deposited through these techniques are shown in Fig. 7. Compared to spin-coated TIPS-pentacene thin films, where crystals are randomly distributed [152], the crystallization of TIPS-pentacene in these advanced techniques is well aligned. In terms of drop casting, by using a tilted angle to guide the flow of the semiconductor solution, the crystallization direction of TIPS-pentacene also follows the flow direction, so that the mobility of the fabricated organic TFTs is improved to around 1 $cm^2V^{-1}s^{-1}$ [141]. However, in most cases, drop casting is a manual process, so repeatability and precise controlling of this process are the main challenges. For blade coating, the crystallization direction is also defined by the movement of the blade, and the mobility of the organic TFTs is over 3 $cm^2V^{-1}s^{-1}$ [147]. In addition, using a micropillar-patterned blade, i.e., fluid-enhanced crystal engineering (FLUENCE), highly aligned single crystals of TIPS-pentacene can be achieved, resulting in a high mobility of 11 $cm^2V^{-1}s^{-1}$ [150]. However, blade coating does not allow patterning at the same time, so a further subtractive process is required.

In order to achieve better material usage and direct patternability, the inkjet printing of TIPS-pentacene has also been reported [98], [104], [144]–[146], [153]–[156]. Though highly crystallized TIPS-pentacene thin films can be achieved, the alignment is hard to control (Figure 7(e)) [146]. To solve this issue, off-center printing has been proposed [156]. Due to the better crystallinity of TIPS-pentacene at the off-center area compared to the center area, the channel area can be covered by well aligned TIPS-pentacene crystals [156]. However, this technique depends on good control of the off-center positions. To enhance the crystallinity of TIPS-pentacene thin films,

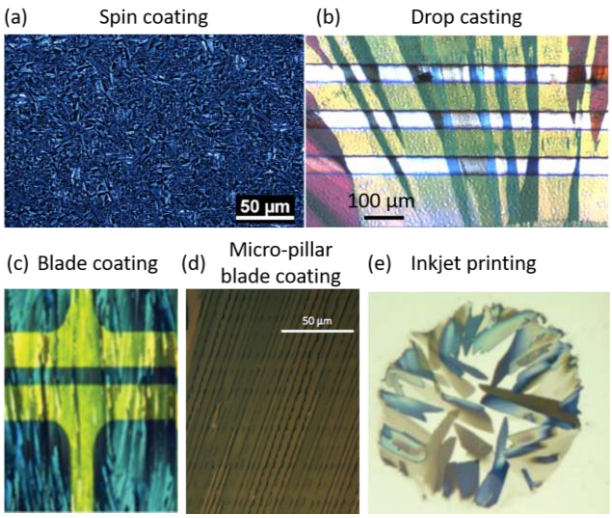

Fig. 7. Optical microscopy images of TIPS-pentacene thin films with various morphologies deposited by different techniques: (a) spin-coating, adapted from [152]; (b) drop casting, adapted from [139]; (c) blade coating, adapted from [147]; (d) solution coating (micro-pillar blade coating), adapted from [150]; (e) inkjet printing, adapted from [146].

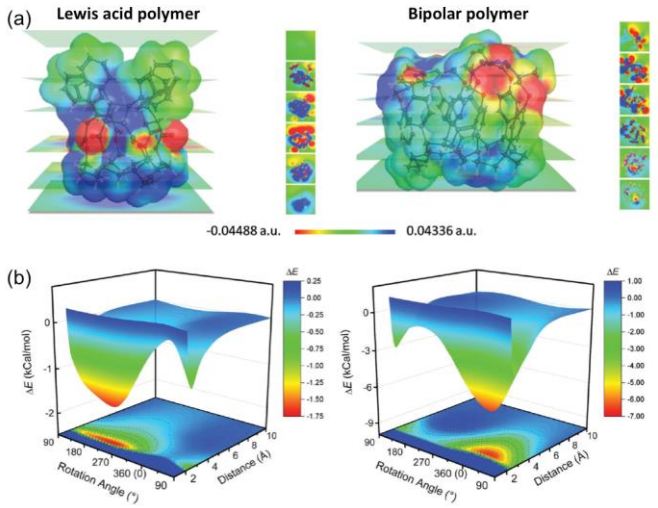

Fig. 8. (a) 3D tomographic comparison of electron densities between a Lewis-acid monopolar polymer, PVC, and a bipolar polymer, PVP. The isosurfaces and tomographic sections are colored by red (electron-rich), green (neutral), and blue (electron-poor). Different atoms in the 3D molecular structures are colored gray (carbon), white (hydrogen), red (oxygen), and blue (nitrogen). (b) The interaction energy (ΔE) when a water molecule approaches PVC and PVP at different rotation angles (from 0° to 360°). Adapted from [96].

polymer binders have been blended into the semiconductor ink, such as polystyrene (PS), poly(α-methyl-styrene) (PαMS), amorphous polycarbonate (APC) [104], [145], [154]. In comparison to the work solely using TIPS-pentacene [98], [144], [146], [153], [157], the TIPS-pentacene/polymer blends facilitate TIPS-pentacene crystallization, and the fabricated organic TFTs exhibit a higher mobility, a higher on/off ratio, and a lower operating voltage.

2) Development of Organic Semiconductors

In addition to significant developments in semiconductor deposition processes, considerable attention has been focused on new solution-processable semiconductor materials. TIPS-pentacene is a derivative of pentacene. In the family of acenes, there are many derivatives that are solution-processable and printable, such as 6,13-bis-(triethylsilylethynyl)pentacene (TES-pentacene) [158] and 2,8-difluoro-5,11-bis(triethylsilylethynyl) anthradithiophene (diF-TES-ADT) [147]. These semiconductor materials, when highly crystallized and well aligned, generally exhibit a mobility of around 1 $cm^2V^{-1}s^{-1}$. In addition to the functionalized acenes, in the recent years, small molecule thiophene-based materials have been popular, such as 2,7-alkyl [1]benzothieno[3,2-b][1]benzothiophene (C8-BTBT) and 2,9-alkyl-dinaphtho [2,3-b:2',3'-f]thieno[3,2-b]thiophene (C10-DNTT). Based on these advanced materials, organic TFTs with a high mobility have been achieved, with a mobility of around 10 $cm^2V^{-1}s^{-1}$ [159], [160], and even as high as 43 $cm^2V^{-1}s^{-1}$ [20]. More recently, a band-like charge transporting material has been developed, 3,11-didecyldinaphtho[2,3-d:2',3'-d']benzo[1,2-b:4,5-b']dithiophene (C10-DNBDT), and nanowire-based organic TFTs exhibit a high mobility of > 17 $cm^2V^{-1}s^{-1}$ [161].

3) Organic Dielectrics

Compared to the significant development of organic semiconductor materials, there has been less interest in advancing organic dielectric materials. In general, organic dielectric materials are polymers. Among polymer dielectrics, the most popular one used in solution-processed organic TFTs is poly(4-vinylphenol) (PVP) [98], [144], [162], [163], due to the straightforward processes of PVP deposition and annealing. CYTOP is another widely used dielectric material, due to its hydrophobicity that prevents water molecules from being polarized or trapped in the dielectric, thus enhancing the stability of organic TFTs [160], [164], [165]. Though good for stability, CYTOP is rarely used in all-solution-processed organic TFTs, since the hydrophobicity of CYTOP eliminates the possibility of depositing functional materials on top of it through solution-based processes. For all-inkjet-printed organic TFTs, most reports used PVP as the dielectric, and the mobility of the printed devices was consistently <0.1 $cm^2V^{-1}s^{-1}$. However, PVP is not a good dielectric material for organic TFTs due to its hydrophilicity that can result in instability. Recently, monopolar dielectrics were proposed as good candidates for all-printed organic TFTs [96], in particular, Lewis-acid monopolar dielectrics which are hydrophobic (Fig. 8), while also allowing good wetting of most organic solvents.

4) All-Printed Organic TFTs

To further reduce the cost and improve the efficiency of organic TFT manufacturing, an all-printed organic TFT device platform is needed. The pioneering work on all-printed organic TFT circuits was reported by Sirringhaus et al. using all polymer materials in 2000. However, the transistors demonstrated a low field effect mobility of 0.02 $cm^2V^{-1}s^{-1}$ and a high operating voltage of 20 V. To improve mobility, researchers replaced the polymer semiconductor by a small molecule semiconductor, typically TIPS-pentacene, which tended to demonstrate a higher mobility [98], [104], [144]–[146], [153]–[156]. However, most works on all-printed organic TFTs based on small molecules also demonstrated low mobilities of ~0.01 $cm^2V^{-1}s^{-1}$ and high operating voltages of > 20 V.

In 2016, Feng et al. controlled the printing processes to reduce semiconductor/dielectric interface trap density and

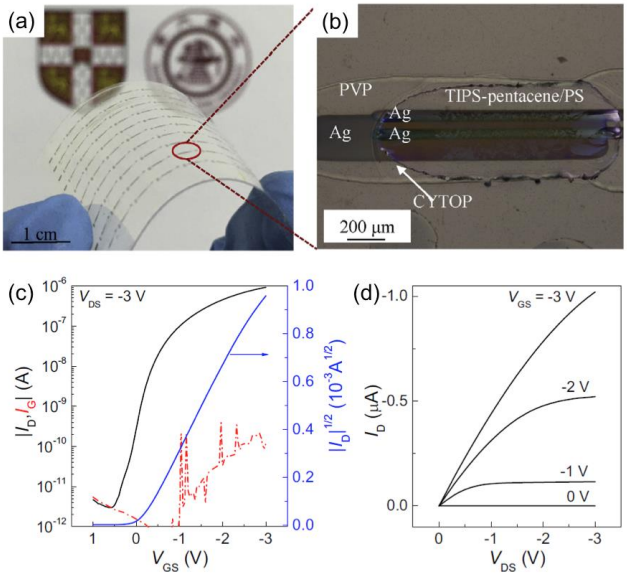

Fig. 9. (a) Photograph of the low-voltage all-inkjet-printed organic TFTs. (b) Polarized optical micrograph of the fabricated device. (c, d) Measured electrical characteristics of the fabricated device: (c) transfer characteristics (I_D-V_{GS}) and (d) output characteristics (I_D-V_{DS}). Adapted from [11].

achieved low-voltage all-inkjet-printed organic TFTs, with a mobility of 0.26 $cm^2V^{-1}s^{-1}$ and an operating voltage of 3 V (see Fig. 9) [11]. However, the organic TFTs used hydrophilic PVP as the dielectric, which resulted in significant threshold voltage shift during bias stress [166]. To enhance all-printed organic TFT bias stress stability, Jiang et al. used a Lewis-acid monopolar dielectric, i.e., polyvinyl cinnamate (PVC), and the threshold voltage shifts were greatly reduced to 0.11 V under both positive and negative bias stress for 1 hour [96]. More recently, Jiang et al. used C8-BTBT as the semiconductor for all-printed organic TFTs. The printed C8-BTBT films possessed large crystals (of which grain sizes were > 50 μm), and the density of states of the TFTs was reduced (i.e., deep state density was ~10^{14} $cm^{-3}eV^{-1}$) [66]. Due to the large semiconductor crystals and reduced traps, the all-printed organic TFTs demonstrated a high mobility of >1.0 $cm^2V^{-1}s^{-1}$ and a low operating voltage of 1 V. In addition, the transistors exhibited good stability under ambient environment storage with threshold voltage shift of <1 mV over 3 months and as well as under bias stress.

D. Examples of Flexible TFT-Based Biosensors

The current development of e-skin biosensors has been reviewed by Hammock el al. [2], Wang et al. [1], and Jung et al. [3]. Readers are encouraged to refer to these review papers for a detailed understanding of e-skin biosensors. This section focuses on what types of signals are generated by biosensors and how they can be fed into interface circuits.

For e-skin, the most important functions for human-machine interfaces include pressure mapping, heartbeat monitoring, temperature capturing, electrophysiology recording, and ion detection.

Pressure mapping can be implemented by using a pressure-sensitive film integrated with TFT arrays. Someya and his coworkers demonstrated an ultra-lightweight imperceptible pressure sensor array using ultra-thin flexible organic TFTs together with a resistive tactile sensing foil, as seen in Fig. 10(a) [21]. In this type of configuration, the pressure sensor array produced a current change when touched by an object, with a magnitude of ~150 μA, which was a relatively small signal due to the low mobilities of organic TFTs. In contrast, also based on a resistive strain sensor, Wang et al. demonstrated a heartbeat monitor with an intrinsically stretchable organic TFT amplifier, while using a potential divider configuration to generate voltage signals to achieve a large amplitude of >0.2 V (Fig. 10(b)) [6]. Similar to the pressure sensor array, Ren et al. demonstrated a low-operating-power and flexible active-matrix organic TFT temperature sensor array, by using a thermistor in series with a TFT (Fig. 10(c)) [167]. The temperature sensor array exhibited good mapping to a wide range of temperatures,

Table 3. Signal types and circuit requirements for different sensors.

Sensor type	Signal type	Signal range	Frequency (Hz)	Interface circuits
Pressure	Current/ Resistance	<1 mA	<10	TIA/VA
Temperature	Current	<1 μA	<1	TIA
Electro-physiology	Voltage	<1 mV	<100	VA
Ion	Voltage/ Capacitance	<60 mV/dec	<1	ISFET+TIA

N.B.: TIA: transconductance amplifier; VA: voltage amplifier.

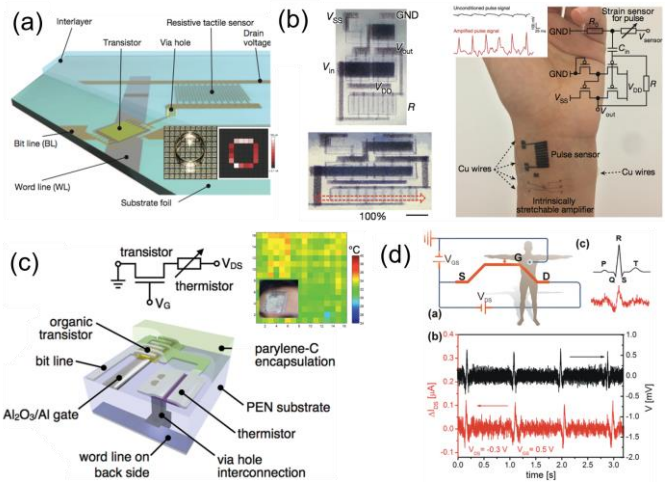

Fig. 10. Examples of flexible TFT-based biosensors. (a) An ultra-lightweight imperceptible pressure sensor array using ultra-thin flexible organic TFTs for pressure mapping, adapted from [21]. (b) An intrinsically stretchable organic TFT amplifier integrated with a resistive sensor for heartbeat monitoring, adapted from [6]. (c) A low-operating-power and flexible active-matrix organic TFT temperature sensor array with a thermistor for temperature capturing, adapted from [167]. (d) Electrocardiogram (ECG) recording using an organic electrochemical transistor, adapted from [28].

i.e., from 20 to 100 °C, but the current change was less than 1 μA. For this small current signal, a low-noise trans-impedance amplifier (TIA) close to the sensor is needed for real application; otherwise, the small current may easily spread out and/or be affected by the noise when transmitting through a long wire.

In terms of electrophysiology recording, the signals can be directly captured by thin-film amplifiers, in contrast to that of pressure mapping and temperature capturing which require tactile sensors. Electrophysiological signals are essentially voltage signals of which the amplitudes are less than 1 mV, and therefore high gain amplifiers are required for capturing these signals with a high sensitivity. Campana et al. used an organic electrochemical transistor that provided larger transconductance for electrocardiogram (ECG) recording (Fig. 10(d)) [28]. However, the recorded current signals were very noisy. Rather than using a transconductance amplifier, Sekitani et al. demonstrated ECG recording on a rat's heart using a high-gain voltage amplifier, providing clear output signals [168]. Besides ECG to record signals from hearts, one can also capture electrophysiological signals from the brain (electroencephalography, EEG), eyes (electrooculography, EOG), muscles (electromyography, EMG), etc., which are also very useful for e-skin or other human/humanoid applications.

Ion detection on e-skin is useful to analyze sweat compositions and their concentrations. There is a specific family of electronic devices for ion detection known as ion-sensitive field effect transistors (ISFETs). Different from the aforementioned biosensors, ISFETs require a gate or a gate dielectric that is ion-sensitive. A common example is pH sensors, which are proton-sensitive. In combination with a functionalized material on the gate or gate dielectric, ISFETs can be selective towards other ions, such as sodium and potassium. The mechanism of an ISFET is that an interface potential is established by the solid/electrolyte interface ions and is modulated by the different concentrations of ions, with a theoretical maximum sensitivity of 60 mV per pH change or per

decade of ion concentration change. Due to the nature of the transistor as a current device, a TIA is also required for ion detection.

For these examples of e-skin biosensors, the frequency requirement is not demanding. It is obvious that activity based on human touch, body temperature change, and ion level change in sweat are slow, i.e., less than 10 Hz. In addition, electrophysiology signals are also in low frequencies of < 100 Hz [169]. Therefore, for e-skin sensor interfaces, a relatively small bandwidth of 100 Hz is enough for most interfacing analog front-end circuits.

IV. Ultralow Power TFTs

To reduce the power consumption of TFTs, it is important to reduce both their operating voltage and current, since power is the product of voltage and current. Here, we discuss steepening the subthreshold slope and subthreshold operation to reduce the operating voltage and current, respectively. Then, we introduce Schottky-barrier subthreshold TFTs, which have geometry-independent electrical characteristics and are promising to accommodate the large variation in printed TFTs. In addition to low power, other requirements for e-skin sensor interfaces that should be taken into account during low power TFT and circuit design are discussed.

A. Subthreshold Slope Steepening

The operating voltage of TFTs can be reduced by steepening the subthreshold slope (*SS*). The subthreshold slope is a term to describe how efficiently a transistor switches from the off-state to the on-state with regard to gate voltage, and quantitatively, how much gate voltage is required to change one order in the magnitude of the drain current, in the unit of volt/decade, or V/dec. The subthreshold slope can be experimentally extracted from the following expression:

$$SS = \frac{\partial V_{GS}}{\partial \ln(I_{DS})} \tag{1}$$

For low-voltage TFTs, their subthreshold slope should be small or steep.

To minimize subthreshold slope, we need to understand its boundary and factors. In theory, the subthreshold slope can be expressed as

$$SS = \ln(10)\frac{k_B T}{q}\left(1 + \frac{q^2 D_t}{C_i}\right) \tag{2}$$

where k_B is Boltzmann's constant, T is the absolute temperature, q is the elementary charge, D_t the defect trap density, and C_i the unit-area gate dielectric capacitance. As seen from Eq. 2, $\ln(10)k_BT/q$ is constant at a certain temperature. For example, given T = 300 K, the theoretical limit of *SS* is 60 mV/dec. To reduce *SS*, D_t should be small, or C_i should be large.

1) Large gate dielectric capacitance

A large unit-area gate dielectric capacitance can be achieved with a thinner dielectric layer or using a high-*k* dielectric material. Hagen et al. packed self-assembled monolayers (~2.1 nm) on plasma treated aluminum oxide (~3.8 nm) as an ultra-thin dielectric for organic TFTs [170], providing a large C_i of 0.7 μF/cm^2. This C_i was about 10~100 times large than normal ones in organic TFTs. Therefore, the subthreshold slope of the organic TFTs was reduced to ~100 mV/dec and the operating voltage was 3 V. In addition, a large C_i was also achieved by Li et al. by using a high-*k* relaxor ferroelectric polymer dielectric material, i.e., poly(vinylidene fluoride-trifluoroethylene-chlorofloroethylene) (P(VDF-TFE-CFE), with k > 60 at room temperature), providing capacitance of about 330 nF/cm^2 at low frequencies [171]. Thus, the fabricated organic TFTs demonstrated a steep subthreshold slope of 97 mV/dec and a low operating voltage of 3V. In addition, ion gel gate dielectrics are also a group of high-*k* materials. By using ion gel dielectrics, a large C_i was obtained around 20 μF/cm^2, and the subthreshold slope was steepened to 100 mV/dec [137].

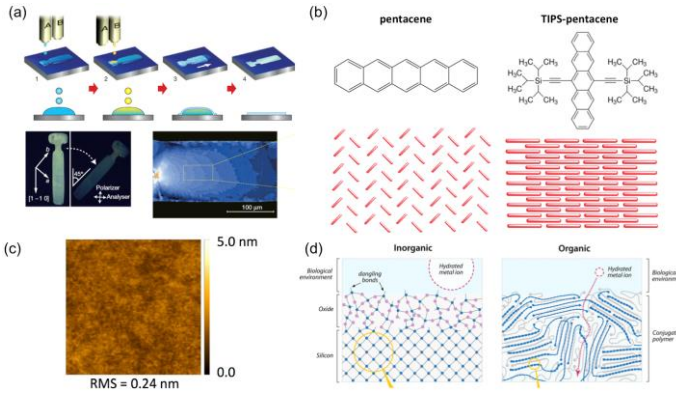

Fig. 11. Reduce defects in organic TFTs. (a) Inkjet printing of single-crystal semiconductor films, adapted from [159]. (b) Molecular packing motifs in organic crystals, with examples of pentacene in herringbone packing (face-to-edge) without π-π overlap (face-to-face) between adjacent molecules and TIPS-pentacene in lamellar motif, 2-D π-stacking, adapted from [94]. (c) Surface roughness of inkjet-printed polymer dielectric, adapted from [11]. (d) Schematics of an inorganic semiconductor, silicon, and an organic semiconductor, PEDOT, at the interface, adapted from [110].

Although these two methods have been effective in reducing operating voltages for vacuum-processed and semi-solution-processed organic TFTs, they can induce additional issues for printed organic TFTs. The ultra-thin gate dielectrics require smooth gate surfaces to ensure good coverage over the gate electrode; otherwise, they can induce large gate leakage current, thus resulting in low drain current on/off ratio and low fabrication yield [11], [97]. However, printed gate electrodes can be rougher than vacuum-deposited electrodes [66]. Therefore, to use ultra-thin gate dielectrics, printed gate electrodes with better surface quality need to be further investigated and developed. For high-*k* dielectrics, organic TFTs could experience a semiconductor/dielectric interface dipole disorder induced by the strong dipole of high-*k* materials [138], thus resulting in the instability of organic TFTs. To avoid this issue, Guo and his coworkers demonstrated a high-*k*/low-*k* bilayer gate dielectric to steepen the subthreshold slope of all-solution-processed organic TFTs, while maintaining good device stability [101], [172], [173]. In the bilayer structure, the high-*k* dielectric was used to enlarge C_i, and the low-*k* dielectric was used as the semiconductor/dielectric interface to avoid dipole disorder.

2) Reduced trap density

Apart from using a large C_i, an alternative way is to reduce D_t. D_t can be affected by defects in the bulk of the semiconductor (e.g., grain boundaries and stacking faults) and at the interface between the semiconductor and dielectric (e.g., interface roughness and dangling bonds) [140], [141].

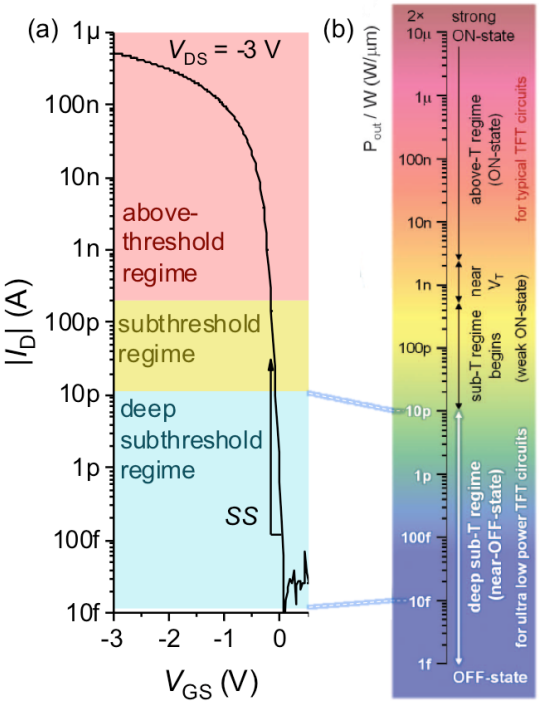

Fig. 12. (a) Electrical transfer characteristics of a TFT, showing different operation regimes. (b) Conceptual color bar of TFT power consumption normalized with channel width for 1 V supply, adapted from [38].

Grain boundaries can be minimized by enhancing the crystallinity of semiconductors. To this end, inkjet printing of single-crystal organic semiconductor films has been reported, using an antisolvent crystallization technique [159]. A larger amount of antisolvent was printed first followed by a smaller amount of semiconductor ink, which triggered the formation of uniform single-crystal thin films that grow at the liquid/air interfaces, as shown in Fig. 11(a). The same technique was also demonstrated to spray print organic semiconductor single crystals [93]. Stacking faults exist in organic semiconductors whose molecular organization is in a herringbone (edge-to-face) pattern (e.g., pentacene, Fig. 11(b)), which impedes charge carrier transport [174]. Functionalized pentacene with side chains was therefore synthesized to achieve face-to-face molecular stacking [88], [175]. By using TIPS-pentacene blended with PS, Guo et al. demonstrated low-voltage organic TFTs with reduced trap density [176]–[178]. These functionalization methods were also applicable to other organic semiconductors, such as BTBT [179], DNTT [180], and dithieno[2,3-d;2′3′-d′]benzo[1,2-b;4,5-b′] dithiophene (DTBDT) [181]. In addition, blending these functionalized thiophene-based semiconductors with PS also demonstrated reduced trap density [20], [99]. Besides symmetric functionalization, Hanna et al. developed an asymmetrically functionalized BTBT-based semiconductor, 2-decyl-7-phenyl-[1] BTBT (Ph-BTBT-10), which forms highly ordered liquid crystals with post-annealing at 120 °C, and the fabricated TFTs have a steep subthreshold slope of 78 mV/dec [182], [183].

Semiconductor/dielectric interface should be smooth to avoid a scattering effect, thereby suppressing defect states at the interface [11], [96], [176]. Regarding dangling bonds, organic materials have an advantage over inorganic materials. Organic materials are van der Waals bonded, so theoretically, there are no dangling bonds; however, inorganic materials are covalently bonded, and therefore, at the interface where one phase of material terminates, dangling bonds prevail (Fig. 11(d)) [110].

Recently, by considering and suppressing all the factors that induce defects, all-inkjet-printed organic TFTs with a subthreshold slope approaching the theoretical limit of 60.2 mV/dec were demonstrated [66], as seen in Fig. 12(a). Such a steep subthreshold slope allows for a low operating voltage of sub-1 V.

B. Subthreshold Operation

One of the most effective ways of reducing the operating current is to operate the transistor in the weak inversion mode, i.e., in the subthreshold regime, as shown in Fig. 12. In silicon CMOS devices, the subthreshold operation was intensively researched in the 1970s [12]–[14], and this led to the most successful low-power designs in electronics, i.e., the electronic watch industry. Despite the success of the subthreshold operation in CMOS, the counterpart for TFTs has not been intensively studied until recently by Nathan and his coworkers [38], [66], [184].

For TFTs operated in the subthreshold regime, the current voltage characteristics can be expressed as [184]

$$I_{DS} = I_{ref} \exp\left(-\frac{V_{GS} - V_T}{SS/\ln(10)}\right) \quad (3)$$

where I_{ref} is the effective subthreshold reference current at V_T. As seen in Eq. 3, the subthreshold drain current exponentially decreases with V_{GS}, thus effectively reducing the operating current and power consumption. As shown in Fig. 12, the power consumption of subthreshold TFTs can be > 10^6 times lower than the above-threshold operation, enabling ultra-low power circuit with a power consumption of < 1nW [38].

Apart from the benefit of low power consumption, other parameters need to be considered for subthreshold operation for e-skin sensor interfaces.

1) Transconductance and transconductance efficiency

Transconductance and transconductance efficiency. The transconductance two of the most important metrics, defined as

$$g_m = \frac{\partial I_{DS}}{\partial V_{GS}} \quad (4)$$

characterizes the dependence of the output drain current on the input gate voltage. In general, the g_m is a positively proportional function to I_{DS}. Therefore, to characterize the efficiency of current/voltage amplification, transconductance efficiency is introduced and defined as g_m/I_{DS}, which can be regarded as a normalized transconductance by the current through the device.

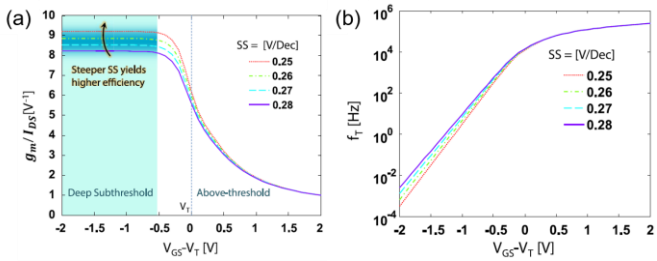

Fig. 13. (a) g_m/I_{DS} from deep subthreshold to above threshold regions. The value reaches a maximum at deep-subthreshold region and increases with steeper SS. (b) Cut-off frequency vs. voltage bias for different *SS*. Adapted from [184].

In order to achieve large transconductance at low power, g_m/I_{DS} should be high.

The transconductance efficiency of a TFT in the above-threshold and subthreshold regimes can be expressed as [184]

$$\frac{g_m}{I_{DS}} = \begin{cases} \dfrac{2+\alpha}{V_{GS}-V_T}, \text{(above threshold)} \\ \dfrac{\ln(10)}{SS}, \text{(subthreshold)} \end{cases} \quad (5)$$

where α is the power law coefficient in the TFT model (α = 0 for the case of MOSFET) [55], [185]. As seen in Fig. 13(a), the transconductance efficiency of a TFT decreases from the subthreshold to the above-threshold regime. This indicates better energy efficiency in the deep subthreshold regime. It is also noteworthy that the transconductance efficiency is a constant in the deep subthreshold regime.

2) Intrinsic gain

Intrinsic gain is an important parameter of TFTs for analog applications, since it reflects the highest achievable single stage gain for an amplifier. By introducing the Early voltage, V_A, the intrinsic gain of subthreshold TFTs can be found as

$$A_i = g_m r_O = \frac{V_A \ln(10)}{SS} \quad (6)$$

It can be seen from Eq. 6 that the intrinsic gain of subthreshold TFTs is also a constant, regardless of the gate bias. It also suggests that A_i is inversely proportional to the *SS* of the TFT. By pushing the *SS* to its theoretical limit (60mV/dec), one could, in principle, exceed a gain of 1000 [184]. This has been verified by experiments with printed organic TFTs whose *SS* is 60 mV/dec, exhibiting an intrinsic gain of ~1100 in the subthreshold regime [66].

3) Cut-off Frequency

The low power of subthreshold TFT is achieved with the lowered subthreshold current, which also reduces the speed of the device. The cut-off frequency of a TFT can be theoretically found by [219, 220]

$$f_T = \frac{g_m}{2\pi C_{ov}} \approx \frac{I_{DS} \cdot \ln(10)}{SS \cdot 2\pi C_{ov}} \quad (7)$$

where C_{ov} is the total overlap capacitance. Eq. 7 indicates that f_T is linearly proportional to I_{DS}. Therefore, the operating current cannot be as low as it can be, though lower operating current reduces power and does not affect transconductance efficiency and intrinsic gain. As seen in Fig. 13(b), the cut-off frequency of subthreshold TFTs is low but should be enough for some e-skin applications, where the maximum frequency of human bio-activities is less than 100 Hz. For example, a subthreshold TFT circuit was demonstrated by Jiang et al. to capture human electro-oculography (EOG) and track eye movements, and it has the potential to be used as a human-machine interface in augmented reality (AR) and virtual reality (VR) applications [66].

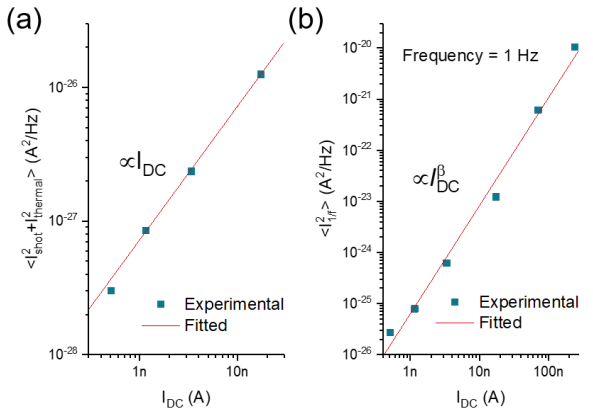

Fig. 14. (a) White noise of subthreshold TFTs as a function of direct current bias. (b) 1/*f* noise at frequency at 1 Hz under different direct current biases. Here, the exponent β is found to be 2.13, in agreement with the theoretical value of 2. Adapted from [66].

4) Noise current

Noise is intrinsic to any device and ultimately limits the minimum detectable signal, especially at low frequencies, where many bio-signals lie (<100 Hz). It is plausible that the subthreshold operating current is low and thus is more vulnerable to noise. However, it was found that the noise current of a subthreshold TFT is a function of its operating current [66]. As the operating current is reduced in the subthreshold, the noise current is also reduced.

There are three well-understood types of noise commonly found in electron devices. These include thermal noise, shot noise and flicker noise [186]. The former two are white (i.e., frequency-independent), and the flicker noise is pink (i.e., inversely proportional to frequency, thus also known as 1/*f* noise). The white components can be expressed as

$$\langle i_{th}^2 \rangle + \langle i_s^2 \rangle = \left(\frac{8k_B T}{3} \frac{\ln(10)}{SS} + 2q \right) I \quad (8)$$

where $\langle i_{th}^2 \rangle$ and $\langle i_s^2 \rangle$ are the thermal noise and shot noise, respectively. The 1/*f* flicker noise can be expressed as

$$\langle i_{1/f}^2 \rangle = K \frac{I^{\beta}}{f^{\alpha}} \quad (9)$$

where *K* is a process-dependent coefficient, α and β are noise parameters (with α=1 and β=2 in theory). Eqs. 8 and 9 indicate that the white noise and flicker noise are proportional to the current through subthreshold TFTs as I and I^2. Experiment results show good agreement with the theoretical expressions, as seen in Fig. 14. With the measured noise, the signal-to-noise ratio was calculated to be over 60 dB, which is possible for many signal detections for e-skin sensors.

C. Schottky-Barrier Subthreshold TFTs

In general, transistors with Schottky semiconductor/metal contacts are not preferred in most electronic applications, in particular TFTs for displays. Here, we discuss the effect of contacts on output resistance and show the advantages of Schottky-barrier contacts on increasing intrinsic gain and accommodating the large variation in printed TFTs.

In ohmic-contact devices, the contact resistance at the semiconductor/metal junction is insignificant compared to the channel resistance, and therefore, the on-state current can be maximized and is linear to *W/L*. However, since transistors mostly operate in the saturation regime, the effective channel length decreases with the increase of V_{DS}, due to the increase of the depletion layer width at the drain side of the channel. This is known as the channel length modulation effect. The I_{DS}-V_{DS} relation can be modeled as [47]

$$I_{DS} = I_{DS,sat}\left(1 + \frac{\Delta L}{L}\right) = I_{DS,sat}(1 + \lambda V_{DS}) \quad (10)$$

where ΔL is the shortened amount of the channel length, λ the channel length modulation parameter. Due to the channel

length modulation effect, the transistor output resistance is not infinite and becomes

$$r_{O,ohmic} = \frac{\partial V_{DS}}{\partial I_{DS}} = \frac{1}{\lambda I_{DS,sat}} \quad (11)$$

In addition, one can see from Eq. 11 that λ is channel length dependent. For printed TFTs, the variation of channel length can be as large as > 10 µm, thus resulting in a large variation in device-to-device output resistance.

In contrast, the Schottky-barrier devices possess a much larger output resistance, since the Schottky-barrier at the source-side semiconductor/metal junction limits the charge carrier injection (see Fig. 18(a)) and thus the channel length modulation effect does not occur. Due to the source-side Schottky-barrier, the I_{DS}-V_{DS} relation can be expressed as

$$I_{DS} = I_{DS,sat}\left(1 - \exp\left(\frac{qV_{DS}}{nk_BT}\right)\right) \quad (12)$$

where n is the ideality factor of the Schottky junction. Therefore, the transistor output resistance is

$$r_{O,Schottky} = n\frac{k_BT}{qV_{DS}}\frac{1}{I_{DS,sat}}\exp\left(-\frac{qV_{DS}}{nk_BT}\right) \quad (13)$$

yielding an infinite value since $-V_{DS}$ is much larger than q/nk_BT in the exponential term. Note that, in Eq. 13, no terms depend on TFT channel length. Therefore, the output resistance of Schottky-barrier subthreshold TFTs can be channel length independent [38], which is ideal for printed TFTs.

V. Compact Models for Circuit Designs

A. Density of States Extraction

The density of states (DOS) is a term that describes the number of allowed states for charge carriers (i.e., electrons and holes) to be occupied per unit energy per unit volume. In an ideal semiconductor, the allowed states exist only in the energy spectroscopy beyond the valance band of the semiconductor and below the conduction band, and there are no allowed states in the sub gap (i.e., between the valance band and conduction band). However, in most TFTs, the semiconductors are typically amorphous or polycrystalline, so there are considerable defects in the semiconductor bulks and at the semiconductor/dielectric interfaces. These defects induce the sub-gap DOS, which charge carriers can occupy but can become easily trapped in.

1) Activation energy-based methods

There are several methods used to extract DOS in TFTs, with the most classic ones using activation energy, developed by Lang et al. [187], Fortunato et al. [188], and Kalb et al [189], [190]. The activation energy (E_a) is defined by

$$\sigma(V_{GS}) = A\exp\left(-\frac{E_a}{k_BT}\right) \quad (14)$$

where $\sigma(V_{GS})$ is the measured field-effect conductivity of a TFT. The activation energy can be calculated by using an Arrhenius plot, with which the DOS can be found by

$$g(E) = \frac{C_i}{q\lambda_{acc}}\left(\frac{\partial E_a}{\partial V_{GS}}\right)^{-1} \quad (15)$$

where λ_{acc} is the accumulation layer thickness. The drawbacks of these methods are that they require temperature dependent measurements and are not suitable for unstable TFTs. This is because unstable TFTs easily alter their electrical characteristics under measurements, and temperature dependent measurements require the measured data at different temperatures, resulting in an unreliable correlation of electrical characteristics to temperatures. Puigdollers et al. conducted temperature measurements on an organic TFT to extract DOS, but they found that the measurement results differed when the TFT was heated up and cooled down to the same temperatures [191].

2) Temperature independent methods

Grünewald et al. proposed a model based on the relationship between the interface electrical field and semiconductor surface potential, i.e., [192]

$$g(E) = \frac{1}{q}\frac{\partial}{\partial\phi_S}\left\{\frac{\varepsilon_i^2}{qt^2\varepsilon_S}(V_{GS} - V_{FB})\left(\frac{\partial\phi_S}{\partial V_{GS}}\right)^{-1}\right\} \quad (16)$$

where ϕ_S is the semiconductor surface potential, V_{FB} is the flatband voltage, t is the dielectric thickness, ε_i and ε_S are the dielectric and semiconductor permittivity, respectively. Eq. 16 does not have a temperature dependent term, and therefore, it is not necessary to conduct temperature measurements on TFTs based on this method of extraction. This method is ideal for TFTs that are not stable, especially organic TFTs. Similar methods with slightly different assumptions were developed to extract DOS in a-Si and AOS TFTs [37], [55]. However, one key drawback of these DOS extraction methods is that the surface potential of semiconductor was assumed to be negligible, which was acceptable in high-voltage TFTs but would not be proper for low-voltage TFTs with a steep subthreshold slope. In the case of low-voltage TFTs, the surface potential of semiconductor is comparable to the gate voltage, and therefore, $C_i(V_{GS} - V_{FB} - \phi_S) \approx C_i(V_{GS} - V_{FB})$.

3) DOS extraction for low-voltage TFTs

To extract the DOS in low-voltage TFTs, the assumption for V_{GS}-ϕ_S approximation needed to be modified. Based on the

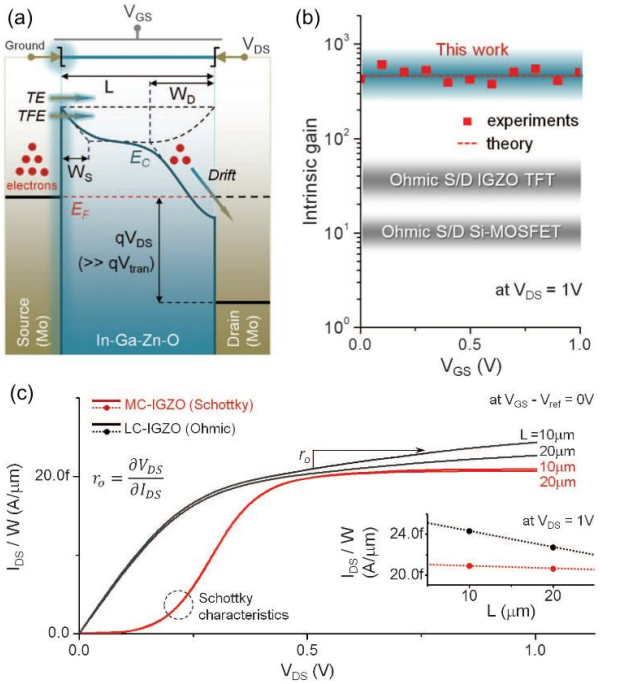

Fig. 15. (a) Operating principle of Schottky-barrier subthreshold TFTs. (b) Intrinsic gain of Schottky-barrier subthreshold TFTs, in comparison with ohmic-TFTs and Si-MOSFET. (c) Channel-length independent characteristics of Schottky-barrier subthreshold TFTs. Adapted from [38].

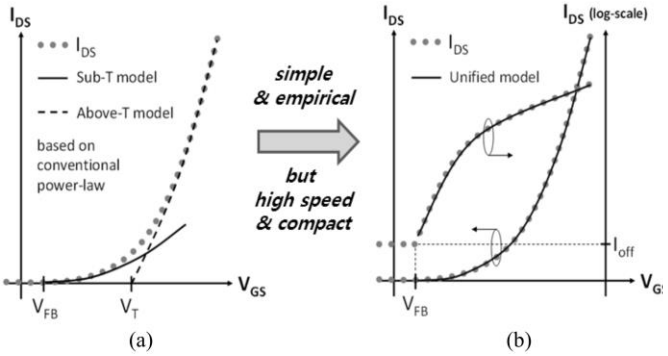

Fig. 16. I_{DS} vs. V_{GS} (a) modeled in different region to join with smoothing function (b) modeled with unified empirical model. Adapted from [185].

temperature-independent extraction method, a modified DOS extraction was developed for universal TFTs, particularly applicable to low-voltage TFTs that are important for ultralow power e-skin. The DOS can be calculated as follows [66]:

$$g(E) = \frac{\partial^2}{\partial {\phi_S}^2}\left\{\frac{C_i^2}{2q\varepsilon_S}(V_{GS} - V_{FB} - \phi_S)^2\right\}\Big|_{E_{F0}+q\phi_S \to E} \quad (17)$$

where E_{F0} is the equilibrium Fermi level. In Eq. 17 the only unknown term is ϕ_S, which can be obtained from a Boltzmann's equation, i.e.,

$$q\phi_S(V_{GS}) = -k_B T \ln\left(\frac{\sigma(V_{GS})}{\mu_b q \lambda_{free} p_{HOMO}}\right) + E_{HOMO} - E_{F0} \quad (18)$$

where μ_b is the band mobility of the semiconductor, λ_{free} is the effective channel thickness of the induced free carrier sheet, and p_{HOMO} is the effective density of free carriers at the highest occupied molecular orbital (HOMO) level.

B. Compact Model

In general, a compact model for circuit simulation should be accurate and converging [185]. As SPICE simulators use the Newton-Raphson method for circuit simulation (or equation solving), the device models created should ensure that the KCL equation sets of a circuit containing TFT devices are solvable using the above method.

Choosing either physical or empirical models for circuit simulation is not an easy task in TFT circuit simulation. While physical models can accurately model the device behavior with potentially minimum fitting parameters, convergence or convergence speed are generally not guaranteed. This is mainly due to the change in dominating physics in different working regions of transistors. To ensure that all working regions of a transistor converge in circuit simulators, smoothing functions are generally added, making the model partially empirical. On the other hand, fully empirical models may sound appealing since functions can be created to intentionally guarantee convergence (making sure the KCL equations are solvable in the Newton-Raphson way). The models, however, tend to have redundant fitting parameters to cover different sizes of transistors and working regions. Recently, Zhao et al. developed a universal compact model with a proper balance between the physical and mathematical approaches [193]. The compact model demonstrated good agreement with the experimental data measured with TFTs of different materials.

As discussed above, for ultra-low power applications, it is beneficial to bias TFTs in the subthreshold region for high transconductance efficiency [184]. Therefore, the working region of interest here is the subthreshold region and the transition region between the above- and sub-threshold regions (to improve the speed when necessary). While the conduction mechanism in the above-threshold region is well studied in most TFT families, less attention has been paid to the subthreshold region. The conduction mechanism in the above region includes trap-limited conduction, percolation conduction, and various range hopping, etc. [194]–[212] for different materials. However, the subthreshold region of TFTs is generally believed to be due to the diffusion current. To model this one should consider connecting the exponential function of the subthreshold region and power-law function of the above-threshold region with smoothing functions or use a unified function to cover both regions in a more empirical way [185], [202]. This is illustrated in Fig. 16. In addition, a DC compact model for subthreshold operated organic TFTs was developed by Guo et al [213]. The modelled transistor current-voltage characteristics fitted well to the experimental results measured from both polymer and small molecule organic TFTs.

One way to test whether a model has good convergence properties is to use the Gummel symmetry test (GST) [203], [214], where both the symmetry and derivatives of the device model are tested to make sure the created model converges in simulators. An example is shown in Fig. 17.

C. Small Signal Model

As for analog sensor interfaces, the frequency response of a device should be accurately captured in a circuit simulator to design the correct gain-phase margin and bandwidth of amplifiers.

A small signal model of a TFT working in the saturation

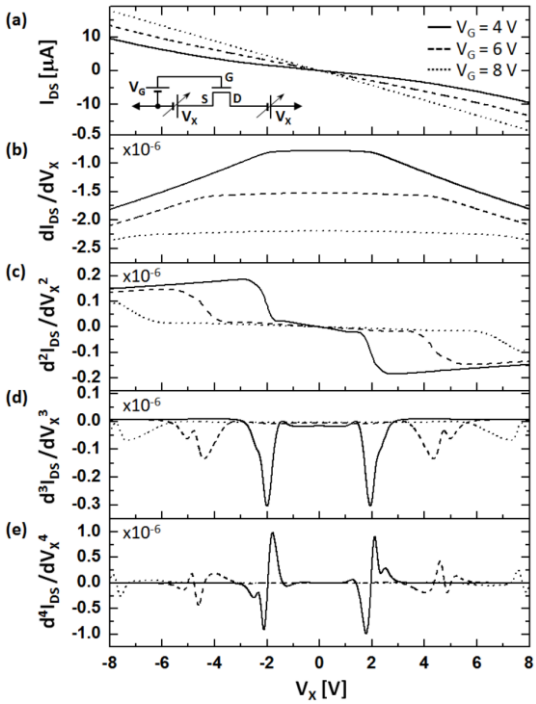

Fig. 17. (a) Calculated I_{DS} vs. V_X of the combined above- and sub-threshold model for different V_{GS} (4, 6, 8V). (b) First, (c) second, (d) third, and (e) fourth derivatives of I_{DS} with respect to V_X. The inset of (a): test circuit configuration of the GST. Adapted from [185].

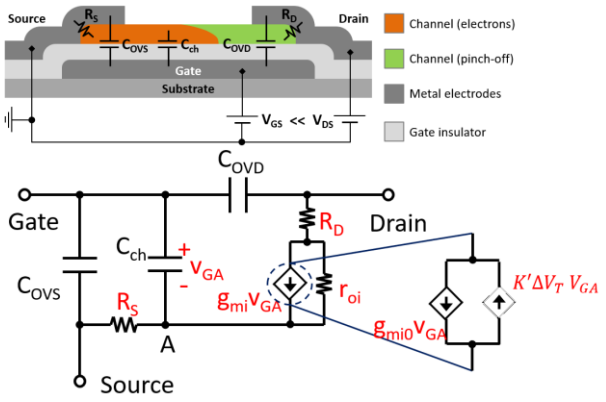

Fig. 18. 3 A small signal model of a TFT considering contact resistance, threshold voltage shift and channel capacitance. Adapted from [215].

region is illustrated in Fig. 18 [215]. In the subthreshold region, a TFT can also work in a saturated manner (especially when used in amplifier applications such as sensor interfaces). However, the parameters can be different due to the channel capacitance not being fully formed. This could lead to the TFT's subthreshold model being equivalent to the generally used MOSFET model in some cases. The major concerns stem from self-aligned architecture in TFT fabrication. In addition, higher sensitivity to threshold voltage shift in this working region may require the V_T shift to be considered in a small signal model.

D. TFT Circuits

With the extracted DOS, compact model, and small signal model, one can design a low-power TFT circuit. Fig. 22 presents an example of an ultralow power circuit with high gain for high-resolution electrophysiology recording. As listed in Table 3, electrophysiology signals are voltage types with a peak-to-peak amplitude of less than 1 mV, and therefore, a high gain voltage amplifier is needed. Fig. 19 demonstrates a common-source amplifier with a peak gain of 260 V/V and maximum circuit power consumption of <1 nW [66]. The circuit was configured to record electro-oculography, which can be useful for eye movement tracking and human-machine interfaces. In addition to single-stage amplifier, a pseudo-CMOS design can improve the performance of amplifier with high gain of >400 V/V [168]. This pseudo-CMOS amplifier with biocompatible electrodes also demonstrated the potential for electrophysiological monitoring.

Besides analog circuits, a digital library for a flexible low-voltage organic TFT technology was established by Elsobky et al., including inverters, NAND gates, flip-flops and shift registers [216]. This library could be the building blocks for more complex circuit and system designs. In addition, CMOS logic circuits have also been reported with flexible n-type and p-type TFTs, demonstrating low operating voltage [217] and short stage delays (<10 ns) [80].

Recently, Bao et al. reported low-voltage high-performance flexible TFTs that can be used both for analog and digital circuits [79]. The amplifier demonstrates a high gain of >200 V/V, and combinational logic gates and ring oscillators showed an average stage delay of 42.7 ± 13.1 ns. Based on these circuits, a self-biased tunable gain amplifier and a sequential circuit of D-type flip-flop were demonstrated.

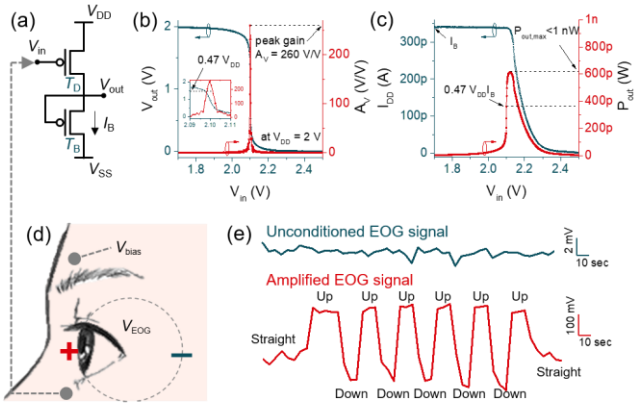

Fig. 19. Ultralow power circuit with a high gain for e-skin interface. (a) Schematic circuit diagram of a common-source amplifier. (b) Measured output voltage (V_{out}) and gain (A_V) as a function of input voltage (V_{in}). (c) Measured operating current (I_{DD}) and power (P_{out}) as functions of V_{in}. (d) Circuit configuration for electro-oculography (EOG) amplification with the amplifier. (e) EOG signal obtained before and after amplification. Adapted from [66].

With this significant development in TFT circuits, we envision the future of TFT systems. There have been a number of reports, such as flexible active-matrix display [218], [219], wearable healthcare monitoring [220], etc.

VI. Conclusion and Outlook

We reviewed different thin-film technologies for e-skin sensor interfaces, comparing their performance attributes from the standpoint of low-cost manufacturing and mechanical flexibility. Although sensors investigated hitherto have been demonstrated to be skin-like, it is not apparent that sensor interface circuits are well-suited for establishing skin-like system-behaviour. Progress on low power organic CMOS circuits and intrinsically flexible/stretchable organic TFTs coupled with recent advances in ultralow power and flexible thin-film electronics would greatly boost further development of e-skin in real-world applications. More importantly, for low-cost manufacturing, we have witnessed significant developments in printing technologies with increased resolution. In the past few years, printed organic TFTs have been demonstrated to operate at voltage. These developments are significantly advancing the printed electronics area.

We also reviewed different sensor examples and compared different the signal types along with the required and compatible interface circuits. By reducing both operating voltage and operating current, the power consumption of interfaces can be as low as or even less than 1 nW. Finally, we reviewed TFT compact models, with which ultralow power e-skin sensor interface circuits have been designed and demonstrated. Indeed, with use of compact modeling for circuit simulation, we will see the advent of low-cost TFT-based sensor interfaces as a high-performance building block for analog front-end circuits.

The ultralow power design for sub-nW sensor interfaces presented here can potentially allow use of energy acquired from micro-harvesters (of the order of μJ/cycle) to enable batteryless operation. This will significantly boost the deployment of e-skin with bio-signal amplification and processing rather than just discrete functional circuit blocks.

REFERENCES

[1] X. Wang, L. Dong, H. Zhang, R. Yu, C. Pan, and Z. L. Wang, "Recent Progress in Electronic Skin," *Adv. Sci.*, vol. 2, no. 10, pp. 1–21, 2015.

[2] M. L. Hammock, A. Chortos, B. C. K. K. Tee, J. B. H. H. Tok, and Z. Bao, "The evolution of electronic skin (E-Skin): A brief history, design considerations, and recent progress," *Adv. Mater.*, vol. 25, no. 42, pp. 5997–6038, 2013.

[3] Y. H. Jung, B. Park, J. U. Kim, and T. il Kim, "Bioinspired Electronics for Artificial Sensory Systems," *Adv. Mater.*, vol. 1803637, pp. 1–22, 2018.

[4] R. Dahiya, "Electronic skin," *Proc. 2015 18th AISEM Annu. Conf. AISEM 2015*, pp. 1–4, 2015.

[5] C. García Núñez, L. Manjakkal, and R. Dahiya, "Energy autonomous electronic skin," *npj Flex. Electron.*, vol. 3, no. 1, 2018.

[6] S. Wang *et al.*, "Skin electronics from scalable fabrication of an intrinsically stretchable transistor array," *Nature*, vol. 555, no. 7694, pp. 83–88, 2018.

[7] W. Gao *et al.*, "Fully integrated wearable sensor arrays for multiplexed in situ perspiration analysis," *Nature*, vol. 529, no. 7587, pp. 509–514, 2016.

[8] H. Nishide and K. Oyaizu, "Toward Flexible Batteries," *Science (80-.).*, vol. 319, pp. 737–738, 2008.

[9] P. D. Mitcheson, E. M. Yeatman, G. K. Rao, A. S. Holmes, and T. C. Green, "Energy harvesting from human and machine motion for wireless electronic devices," *Proc. IEEE*, vol. 96, no. 9, pp. 1457–1486, 2008.

[10] H. Sirringhaus *et al.*, "High-resolution inkjet printing of all-polymer transistor circuits.," *Science (80-.).*, vol. 290, no. 2000, pp. 2123–2126, 2000.

[11] L. Feng, C. Jiang, H. Ma, X. Guo, and A. Nathan, "All ink-jet printed low-voltage organic field-effect transistors on flexible substrate," *Org. Electron.*, vol. 38, pp. 186–192, 2016.

[12] E. Vittoz and J. Fellrath, "CMOS analog integrated circuits based on weak inversion operation," *IEEE J. Solid-State Circuits*, vol. 12, no. 3, pp. 224–231, 1977.

[13] M. B. B. Barron, "Low level currents in insulated gate field effect transistors," *Solid. State. Electron.*, vol. 15, pp. 293–302, 1972.

[14] L. Magnelli, F. Crupi, P. Corsonello, C. Pace, and G. Iannaccone, "A 2.6 nW, 0.45 v temperature-compensated subthreshold CMOS voltage reference," *IEEE J. Solid-State Circuits*, vol. 46, no. 2, pp. 465–474, 2011.

[15] L. Shepherd and C. Toumazou, "Weak Inversion ISFETs for ultra-low power biochemical sensing and real-time analysis," *Sensors Actuators, B Chem.*, vol. 107, no. 1 SPEC. ISS., pp. 468–473, 2005.

[16] G. Giustolisi, G. Palumbo, M. Criscione, and F. Cutri, "A low-voltage low-power voltage reference based on subthreshold MOSFETs," *IEEE J. Solid-State Circuits*, vol. 38, no. 1, pp. 151–154, 2003.

[17] K. Nomura, H. Ohta, A. Takagi, T. Kamiya, M. Hirano, and H. Hosono, "Room-temperature fabrication of transparent flexible thin-film transistors using amorphous oxide semiconductors," *Nature*, vol. 432, no. 7016, pp. 488–492, 2004.

[18] S. Lee, S. Jeon, R. Chaji, and A. Nathan, "Transparent semiconducting oxide technology for touch free interactive flexible displays," *Proc. IEEE*, vol. 103, no. 4, pp. 644–664, 2015.

[19] R. Martins *et al.*, "Complementary metal oxide semiconductor technology with and on paper," *Adv. Mater.*, vol. 23, no. 39, pp. 4491–4496, 2011.

[20] Y. Yuan *et al.*, "Ultra-high mobility transparent organic thin film transistors grown by an off-centre spin-coating method," *Nat. Commun.*, vol. 5, pp. 1–9, 2014.

[21] M. Kaltenbrunner *et al.*, "An ultra-lightweight design for imperceptible plastic electronics," *Nature*, vol. 499, no. 7459, pp. 458–63, 2013.

[22] H. Ebata *et al.*, "Highly Soluble [1]Benzothieno[3,2-b]benzothiophene (BTBT) Derivatives for High-Performance, Solution-Processed Organic Field-Effect Transistors," *J. Am. Chem. Soc.*, vol. 129, no. 51, pp. 15732–15733, 2007.

[23] R. A. Street, "Thin-film transistors," *Adv. Mater.*, vol. 21, no. 20, pp. 2007–2022, 2009.

[24] A. Nathan *et al.*, "Flexible electronics: The next ubiquitous platform," *Proc. IEEE*, vol. 100, no. SPL CONTENT, pp. 1486–1517, 2012.

[25] J. F. Wager, "Transparent electronics," *Science (80-.).*, vol. 300, pp. 1245–1246, 2003.

[26] H. Keum, M. Mccormick, P. Liu, Y. Zhang, and F. G. Omenetto, "Epidermal Electronics," *Science (80-.).*, vol. 333, no. September, pp. 838–844, 2011.

[27] T. Someya, Z. Bao, and G. G. Malliaras, "The rise of plastic bioelectronics," *Nature*, vol. 540, no. 7633, pp. 379–385, 2016.

[28] A. Campana, T. Cramer, D. T. Simon, M. Berggren, and F. Biscarini, "Electrocardiographic recording with conformable organic electrochemical transistor fabricated on resorbable bioscaffold," *Adv. Mater.*, vol. 26, no. 23, pp. 3874–3878, 2014.

[29] D. Khodagholy *et al.*, "In vivo recordings of brain activity using organic transistors," *Nat. Commun.*, vol. 4, 2013.

[30] Y. Kim *et al.*, "A bioinspired flexible organic artificial afferent nerve," *Science (80-.).*, vol. 360, no. 6392, pp. 998–1003, 2018.

[31] M. Singh, H. M. Haverinen, P. Dhagat, and G. E. Jabbour, "Inkjet printing-process and its applications," *Adv. Mater.*, vol. 22, no. 6, pp. 673–685, 2010.

[32] K. Fukuda *et al.*, "Fully-printed high-performance organic thin-film transistors and circuitry on one-micron-thick polymer films," *Nat. Commun.*, vol. 5, no. May, p. 4147, 2014.

[33] T. Sekitani, U. Zschieschang, H. Klauk, and T. Someya, "Flexible organic transistors and circuits with extreme bending stability," *Nat. Mater.*, vol. 9, no. 12, pp. 1015–1022, 2010.

[34] J. Xu *et al.*, "Highly stretchable polymer semiconductor films through the nanoconfinement effect," *Science (80-.).*, vol. 355, no. January, pp. 59–64, 2017.

[35] X. Cheng, S. Lee, R. Chaji, and A. Nathan, "Device-circuit interactions and impact on TFT circuit-system design," *IEEE J. Emerg. Sel. Top. Circuits Syst.*, vol. 7, no. 1, pp. 71–80, 2017.

[36] S. Lee, S. Jeon, and A. Nathan, "Modeling sub-threshold current-voltage characteristics in thin film transistors," *J. Disp. Technol.*, vol. 9, no. 11, pp. 883–889, 2013.

[37] S. Lee and A. Nathan, "Conduction Threshold in Accumulation-Mode InGaZnO Thin Film Transistors," *Sci. Rep.*, vol. 6, no. October 2015, pp. 1–9, 2016.

[38] S. Lee and A. Nathan, "Subthreshold Schottky-barrier thin-film transistors with ultralow power and high intrinsic gain," *Science (80-.).*, vol. 354, no. 6310, pp. 302–304, 2016.

[39] Y. Liu, M. Pharr, and G. A. Salvatore, "Lab-on-Skin: A Review of Flexible and Stretchable Electronics for Wearable Health Monitoring," *ACS Nano*, vol. 11, no. 10, pp. 9614–9635, 2017.

[40] T. Mano *et al.*, "Printed Organic Transistor-Based Enzyme Sensor for Continuous Glucose Monitoring in Wearable Healthcare Applications," *ChemElectroChem*, vol. 5, no. 24, pp. 3881–3886, 2018.

[41] T. Someya *et al.*, "Conformable, flexible, large-area networks of pressure and thermal sensors with organic transistor active matrixes," *Proc. Natl. Acad. Sci.*, vol. 102, no. 35, pp. 12321–12325, 2005.

[42] M.-M. Laurila *et al.*, "A fully printed ultra-thin charge amplifier for on-skin biosignal measurements," *IEEE J. Electron Devices Soc.*, no. May, 2019.

[43] M. C. Caccami, M. P. Hogan, M. Alfredsson, G. Marrocco, and J. C. Batchelor, "A Tightly Integrated Multilayer Battery Antenna for RFID Epidermal Applications," *IEEE Trans. Antennas Propag.*, vol. 66, no. 2, pp. 609–617, 2018.

[44] X. Huang *et al.*, "Epidermal radio frequency electronics for wireless power transfer," *Microsystems Nanoeng.*, vol. 2, no. June, pp. 1–9, 2016.

[45] S. K. Ameri *et al.*, "Imperceptible electrooculography graphene sensor system for human–robot interface," *npj 2D Mater. Appl.*, vol. 2, no. 1, pp. 1–7, 2018.

[46] R. A. Street, *Hydrogenated Amorphous Silicon*. Cambridge: Cambridge University Press, 1991.

[47] S. M. Sze, *Physics of Semiconductor Devices*, 2nd ed. Hoboken, NJ, USA: Wiley, 1981.

[48] Y. Yamamoto and A. T. Voutsas, "Technology trend of AMLCDs for mobile applications," *ECS Trans.*, vol. 3,

no. 8, pp. 11–22, 2006.
[49] Y. Kuo, “Thin Film Transistor Technology—Past, Present, and Future,” *Electrochem. Soc. Interface*, vol. 22, no. 1, pp. 55–61, 2013.
[50] Y. Kuo and P. M. Kozlowski, “Polycrystalline silicon formation by pulsed rapid thermal annealing of amorphous silicon,” *Appl. Phys. Lett.*, vol. 69, no. 8, pp. 1092–1094, 1996.
[51] Atsushi Kohno, T. Sameshima, N. Sano, M. Sekiya, and M. Hara, “High performance poly-Si TFTs fabricated using pulsed laser annealing and remote plasma CVD with low temperature processing,” *IEEE Trans. Electron Devices*, vol. 42, no. 2, 1995.
[52] R. B. M. Cross and M. M. De Souza, “Investigating the stability of thin film transistors with zinc oxide as the channel layer,” *Annu. Proc. - Reliab. Phys.*, vol. 263513, no. November 2018, pp. 467–471, 2007.
[53] T. Kamiya and H. Hosono, “Material characteristics and applications of transparent amorphous oxide semiconductors,” *NPG Asia Mater.*, vol. 2, no. 1, pp. 15–22, 2010.
[54] Y. Ye, R. Lim, and J. M. White, “High mobility amorphous zinc oxynitride semiconductor material for thin film transistors,” *J. Appl. Phys.*, vol. 106, no. 7, 2009.
[55] S. Lee, A. Nathan, Y. Ye, Y. Guo, and J. Robertson, “Localized Tail States and Electron Mobility in Amorphous ZnON Thin Film Transistors,” *Sci. Rep.*, vol. 5, pp. 1–9, 2015.
[56] Y. Ogo *et al.*, “P -channel thin-film transistor using p -type oxide semiconductor, SnO,” *Appl. Phys. Lett.*, vol. 93, no. 3, pp. 1–4, 2008.
[57] L. Liao *et al.*, “Multifunctional CuO nanowire devices: P-type field effect transistors and CO gas sensors,” *Nanotechnology*, vol. 20, no. 8, 2009.
[58] J. Sheng, E. J. Park, B. Shong, and J. S. Park, “Atomic Layer Deposition of an Indium Gallium Oxide Thin Film for Thin-Film Transistor Applications,” *ACS Appl. Mater. Interfaces*, vol. 9, no. 28, pp. 23934–23940, 2017.
[59] J. S. Park, K. Kim, Y. G. Park, Y. G. Mo, H. D. Kim, and J. K. Jeong, “Novel ZrInZnO thin-film transistor with excellent stability,” *Adv. Mater.*, vol. 21, no. 3, pp. 329–333, 2009.
[60] N. Mitoma *et al.*, “Stable amorphous In2O3-based thin-film transistors by incorporating SiO2to suppress oxygen vacancies,” *Appl. Phys. Lett.*, vol. 104, no. 10, pp. 5–10, 2014.
[61] S. Aikawa, T. Nabatame, and K. Tsukagoshi, “Effects of dopants in InOx-based amorphous oxide semiconductors for thin-film transistor applications,” *Appl. Phys. Lett.*, vol. 103, no. 17, pp. 1–6, 2013.
[62] T. Kizu *et al.*, “Low-temperature processable amorphous In-W-O thin-film transistors with high mobility and stability,” *Appl. Phys. Lett.*, vol. 104, no. 15, pp. 1–6, 2014.
[63] E. M. C. Fortunato *et al.*, “High mobility indium free amorphous oxide thin film transistors,” *Appl. Phys. Lett.*, vol. 92, no. 22, pp. 90–93, 2008.
[64] X. Yang, S. Jiang, J. Li, J.-H. Zhang, and X.-F. Li, “Improvement of the long-term stability of ZnSnO thin film transistors by tungsten incorporation using a solution-process method,” *RSC Adv.*, vol. 8, pp. 20990–20995, 2018.
[65] H. J. Jeong, H. M. Lee, K. C. Ok, J. J. S. Park, and J. J. S. Park, “Supreme performance of zinc oxynitride thin film transistors: Via systematic control of the photo-thermal activation process,” *J. Mater. Chem. C*, vol. 6, no. 19, pp. 5171–5175, 2018.
[66] C. Jiang, H. W. Choi, X. Cheng, H. Ma, D. Hasko, and A. Nathan, “Printed subthreshold organic transistors operating at high gain and ultralow power,” *Science (80-.).*, vol. 363, no. 6428, pp. 719–723, 2019.
[67] T. Shimoda *et al.*, “Solution-processed silicon films and transistors,” *Nature*, vol. 440, no. 7085, pp. 783–786, 2006.
[68] E. Menard, R. G. Nuzzo, and J. a. Rogers, “Bendable single crystal silicon thin film transistors formed by printing on plastic substrates,” *Appl. Phys. Lett.*, vol. 86, no. 9, pp. 1–3, 2005.
[69] E. Menard, K. J. Lee, D. Y. Khang, R. G. Nuzzo, and J. a. Rogers, “A printable form of silicon for high performance thin film transistors on plastic substrates,” *Appl. Phys. Lett.*, vol. 84, no. 26, pp. 5398–5400, 2004.
[70] S. Kim, S. Yoon, and H. Kim, “Review of solution-processed oxide thin-film transistors,” *Jpn. J. Appl. Phys.*, vol. 02, 2014.
[71] J. Socratous *et al.*, “Electronic structure of low-temperature solution-processed amorphous metal oxide semiconductors for thin-film transistor applications,” *Adv. Funct. Mater.*, vol. 25, no. 12, pp. 1873–1885, 2015.
[72] H. Faber *et al.*, “Indium oxide thin-film transistors processed at low temperature via ultrasonic spray pyrolysis,” *ACS Appl. Mater. Interfaces*, vol. 7, no. 1, pp. 782–790, 2015.
[73] D. H. Lee, S. Y. Han, G. S. Herman, and C. H. Chang, “Inkjet printed high-mobility indium zinc tin oxide thin film transistors,” *J. Mater. Chem.*, vol. 19, no. 20, pp. 3135–3137, 2009.
[74] Y. Li *et al.*, “All Inkjet-Printed Metal-Oxide Thin-Film Transistor Array with Good Stability and Uniformity Using Surface-Energy Patterns,” *ACS Appl. Mater. Interfaces*, vol. 9, no. 9, pp. 8194–8200, 2017.
[75] S.-Y. Han, D.-H. Lee, G. S. Herman, and C.-H. Chang, “Inkjet-Printed High Mobility Transparent–Oxide Semiconductors,” *J. Disp. Technol.*, vol. 5, no. 12, pp. 520–524, Dec. 2009.
[76] X. Xu, L. Feng, S. He, Y. Jin, and X. Guo, “Solution-processed zinc oxide thin-film transistors with a low-temperature polymer passivation layer,” *IEEE Electron Device Lett.*, vol. 33, no. 10, pp. 1420–1422, 2012.
[77] A. Javey, J. Guo, Q. Wang, M. Lundstrom, and H. Dai, “Ballistic Carbon Nanotube Transistors,” *Nature*, vol. 424, no. August, pp. 654–657, 2003.
[78] D. J. Lipomi *et al.*, “Skin-like pressure and strain sensors based on transparent elastic films of carbon nanotubes,” *Nat. Nanotechnol.*, vol. 6, no. 12, pp. 788–792, 2011.
[79] T. Lei *et al.*, “Low-voltage high-performance flexible digital and analog circuits based on ultrahigh-purity semiconducting carbon nanotubes,” *Nat. Commun.*, vol. 10, no. 1, p. 2161, 2019.
[80] J. Tang *et al.*, “Flexible CMOS integrated circuits based on carbon nanotubes with sub-10 ns stage delays,” *Nat. Electron.*, vol. 1, no. 3, pp. 191–196, 2018.
[81] A. L. Briseno *et al.*, “Perylenediimide nanowires and their use in fabricating field-effect transistors and complementary inverters,” *Nano Lett.*, vol. 7, no. 9, pp. 2847–2853, 2007.
[82] A. L. Briseno, S. C. B. Mannsfeld, S. A. Jenekhe, Z. Bao, and Y. Xia, “Introducing organic nanowire transistors,” *Mater. Today*, vol. 11, no. 4, pp. 38–47, 2008.
[83] B. Radisavljevic and A. Kis, “Mobility engineering and a metal-insulator transition in monolayer MoS_2.,” *Nat. Mater.*, vol. 12, no. 9, pp. 815–20, Sep. 2013.
[84] B. Radisavljevic, a Radenovic, J. Brivio, V. Giacometti, and a Kis, “Single-layer MoS2 transistors.,” *Nat. Nanotechnol.*, vol. 6, no. 3, pp. 147–50, Mar. 2011.
[85] M. Tosun, S. Chuang, H. Fang, A. B. Sachid, M. Hettick, and Y. Lin, “High-Gain Inverters Based on WSe2 Complementary Field-Effect Transistors,” *ACS Nano*, vol. 8, no. 5, pp. 4948–4953, 2014.
[86] H. Fang, S. Chuang, T. C. Chang, K. Takei, T. Takahashi, and A. Javey, “High-performance single layered WSe 2 p-FETs with chemically doped contacts,” *Nano Lett.*, vol. 12, no. 7, pp. 3788–3792, 2012.
[87] V. Podzorov, S. E. Sysoev, E. Loginova, V. M. Pudalov, and M. E. Gershenson, “Single-crystal organic field effect transistors with the hole mobility ∼8 cm2/Vs,” *Appl. Phys. Lett.*, vol. 83, no. 17, pp. 3504–3506, 2003.
[88] J. E. Anthony, J. S. Brooks, D. L. Eaton, and S. R. Parkin, “Functionalized pentacene: Improved electronic properties from control of solid-state order,” *J. Am. Chem. Soc.*, vol. 123, no. 38, pp. 9482–9483, 2001.
[89] M. M. Payne, S. R. Parkin, J. E. Anthony, C. C. Kuo, and T. N. Jackson, “Organic field-effect transistors from solution-deposited functionalized acenes with mobilities as high as 1 cm2/V·s,” *J. Am. Chem. Soc.*, vol. 127, no. 14, pp. 4986–4987, 2005.
[90] M. Kano, T. Minari, and K. Tsukagoshi, “Improvement of subthreshold current transport by contact interface modification in p -type organic field-effect transistors,” *Appl. Phys. Lett.*, vol. 94, no. 14, 2009.
[91] H. Sirringhaus *et al.*, “Two-dimensional charge transport in self-organized, high-mobility conjugated polymers,”

Nature, vol. 401, no. 6754, pp. 685–688, 1999.

[92] D. Venkateshvaran *et al.*, "Approaching disorder-free transport in high-mobility conjugated polymers," *Nature*, vol. 515, no. 7527, pp. 384–388, 2014.

[93] G. P. Rigas, M. M. Payne, J. E. Anthony, P. N. Horton, F. A. Castro, and M. Shkunov, "Spray printing of organic semiconducting single crystals," *Nat. Commun.*, vol. 7, pp. 1–8, 2016.

[94] H. Koezuka, A. Tsumura, and T. Ando, "Field-effect transistor with polythiophene thin film," *Synth. Met.*, vol. 18, no. 1–3, pp. 699–704, 1987.

[95] X. Guo *et al.*, "Current Status and Opportunities of Organic Thin-Film Transistor Technologies," *IEEE Trans. Electron Devices*, vol. 64, no. 5, pp. 1906–1921, 2017.

[96] C. Jiang, H. Ma, D. G. Hasko, X. Guo, and A. Nathan, "A Lewis-Acid Monopolar Gate Dielectric for All-Inkjet-Printed Highly Bias-Stress Stable Organic Transistors," *Adv. Electron. Mater.*, vol. 3, no. 8, p. 1700029, 2017.

[97] E. Sowade *et al.*, "All-inkjet-printed thin-film transistors: manufacturing process reliability by root cause analysis," *Sci. Rep.*, vol. 6, no. April, p. 33490, 2016.

[98] S. H. Lee, M. H. Choi, S. H. Han, D. J. Choo, J. Jang, and S. K. Kwon, "High-performance thin-film transistor with 6,13-bis(triisopropylsilylethynyl) pentacene by inkjet printing," *Org. Electron. physics, Mater. Appl.*, vol. 9, no. 5, pp. 721–726, 2008.

[99] R. Shiwaku *et al.*, "Printed organic inverter circuits with ultralow operating voltages," *Adv. Electron. Mater.*, vol. 3, no. 5, p. 1600557, 2017.

[100] C. Jiang, H. W. Choi, C. Xiang, H. Ma, D. G. Hasko, and A. Nathan, "ultra-low power fully-printed subthreshold organic thin-film transistor with transconductance close to the theoretical limit," *to be Publ.*

[101] J. Zhao, W. Tang, Q. Li, W. Liu, and X. Guo, "Fully Solution Processed Bottom-Gate Organic Field-Effect Transistor with Steep Subthreshold Swing Approaching the Theoretical Limit," *IEEE Electron Device Lett.*, vol. 38, no. 10, pp. 1465–1468, 2017.

[102] T. Sekitani *et al.*, "Bending experiment on pentacene field-effect transistors on plastic films," *Appl. Phys. Lett.*, vol. 86, no. 7, pp. 1–3, 2005.

[103] Y. Guo, G. Yu, and Y. Liu, "Functional organic field-effect transistors," *Adv. Mater.*, vol. 22, no. 40, pp. 4427–4447, 2010.

[104] B. K. C. Kjellander *et al.*, "Optimized circuit design for flexible 8-bit RFID transponders with active layer of ink-jet printed small molecule semiconductors," *Org. Electron. physics, Mater. Appl.*, vol. 14, no. 3, pp. 768–774, 2013.

[105] K. Myny *et al.*, "A thin-film microprocessor with inkjet print-programmable memory," *Sci. Rep.*, vol. 4, pp. 1–6, 2014.

[106] M. Zhang, C. Liao, C. H. C. L. Mak, P. You, C. H. C. L. Mak, and F. Yan, "Highly sensitive glucose sensors based on enzyme-modified whole-graphene solution-gated transistors," *Sci. Rep.*, vol. 5, pp. 1–6, 2015.

[107] B. C.-K. Tee *et al.*, "A skin-inspired organic digital mechanoreceptor," *Science (80-.).*, vol. 350, no. 6258, pp. 313–316, 2015.

[108] J. T. Mabeck and G. G. Malliaras, "Chemical and biological sensors based on organic thin-film transistors," *Anal. Bioanal. Chem.*, vol. 384, no. 2, pp. 343–353, 2006.

[109] P. Gkoupidenis, D. A. Koutsouras, and G. G. Malliaras, "Neuromorphic device architectures with global connectivity through electrolyte gating," *Nat. Commun.*, vol. 8, no. May, pp. 1–8, 2017.

[110] J. Rivnay, R. M. Owens, and G. G. Malliaras, "The rise of organic bioelectronics," *Chem. Mater.*, vol. 26, no. 1, pp. 679–685, 2014.

[111] S. Inal, G. G. Malliaras, and J. Rivnay, "Benchmarking organic mixed conductors for transistors," *Nat. Commun.*, vol. 8, no. 1, pp. 1–6, 2017.

[112] J. Rivnay *et al.*, "High-performance transistors for bioelectronics through tuning of channel thickness," *Sci. Adv.*, vol. 1, no. 4, p. e1400251, 2015.

[113] F. C. Krebs, "Fabrication and processing of polymer solar cells: A review of printing and coating techniques," *Sol. Energy Mater. Sol. Cells*, vol. 93, no. 4, pp. 394–412, 2009.

[114] B. Derby, "Inkjet Printing of Functional and Structural Materials: Fluid Property Requirements, Feature Stability, and Resolution," *Annu. Rev. Mater. Res.*, vol. 40, no. 1, pp. 395–414, 2010.

[115] R. Das, *Printing Equipment for Printed Electronics 2015-2025*. IDTechEx, 2015.

[116] C. M. S. Torres, *Alternative lithography: unleashing the potentials of nanotechnology*. Springer Science & Business Media, 2012.

[117] P. Ma *et al.*, "Fast fabrication of TiO2hard stamps for nanoimprint lithography," *Mater. Res. Bull.*, vol. 90, pp. 253–259, 2017.

[118] M. M. Alkaisi and K. Mohamed, *Three-dimensional patterning using ultraviolet nanoimprint lithography*. INTECH Open Access Publisher, 2010.

[119] D. Lupo, W. Clemens, S. Breitung, and K. Hecker, *OE-A Roadmap for Organic and Printed Electronics*. Springer, 2013.

[120] E. B. Secor, S. Lim, H. Zhang, C. D. Frisbie, L. F. Francis, and M. C. Hersam, "Gravure Printing of Graphene for Large-area Flexible Electronics," *Adv. Mater.*, vol. 26, no. 26, pp. 4533–4538, 2014.

[121] J. M. Ding, A. de la Fuente Vornbrock, C. Ting, and V. Subramanian, "Patternable polymer bulk heterojunction photovoltaic cells on plastic by rotogravure printing," *Sol. Energy Mater. Sol. Cells*, vol. 93, no. 4, pp. 459–464, 2009.

[122] H. Santa-Nokki, J. Kallioinen, T. Kololuoma, V. Tuboltsev, and J. Korppi-Tommola, "Dynamic preparation of TiO2 films for fabrication of dye-sensitized solar cells," *J. Photochem. Photobiol. A Chem.*, vol. 182, no. 2, pp. 187–191, 2006.

[123] T. K. Kololuoma *et al.*, "Towards roll-to-roll fabrication of electronics, optics, and optoelectronics for smart and intelligent packaging," in *Integrated Optoelectronic Devices 2004*, 2004, no. June 2004, p. 77.

[124] D. Deganello, J. A. Cherry, D. T. Gethin, and T. C. Claypole, "Impact of metered ink volume on reel-to-reel flexographic printed conductive networks for enhanced thin film conductivity," *Thin Solid Films*, vol. 520, no. 6, pp. 2233–2237, 2012.

[125] H. Kempa *et al.*, "Complementary ring oscillator exclusively prepared by means of gravure and flexographic printing," *Electron Devices, IEEE Trans.*, vol. 58, no. 8, pp. 2765–2769, 2011.

[126] G. McKerricher, J. G. Perez, and A. Shamim, "Fully inkjet printed RF inductors and capacitors using polymer dielectric and silver conductive ink with through vias," *IEEE Trans. Electron Devices*, vol. 62, no. 3, pp. 1002–1009, 2015.

[127] B. Daemi and L. Mattsson, "Performance evaluation of a micro screen printing installation," pp. 1–9.

[128] J. Noh, S. Kim, K. Jung, J. Kim, S. Cho, and G. Cho, "Fully gravure printed half adder on plastic foils," *IEEE Electron Device Lett.*, vol. 32, no. 11, pp. 1555–1557, 2011.

[129] H. Lan and Y. Ding, "Nanoimprint Lithography," in *Lithography*, M. Wang, Ed. 2010, p. 457.

[130] J. Zaumseil and H. Sirringhaus, "Electron and Ambipolar Transport in Organic Field-Effect Transistors," *Chem. Rev.*, vol. 107, pp. 1296–1323, 2007.

[131] Y.-Y. Noh, N. Zhao, M. Caironi, and H. Sirringhaus, "Downscaling of self-aligned, all-printed polymer thin-film transistors," *Nat. Nanotechnol.*, vol. 2, no. 12, pp. 784–789, 2007.

[132] J. C. Park *et al.*, "High performance amorphous oxide thin film transistors with self-aligned top-gate structure," in *International Electron Devices Meeting, IEDM*, 2009, pp. 191–194.

[133] M. Kaltenbrunner *et al.*, "Ultrathin and lightweight organic solar cells with high flexibility," *Nat. Commun.*, vol. 3, 2012.

[134] J. A. Rogers, T. Someya, and Y. Huang, "Materials and mechanics for stretchable electronics," *Science (80-.).*, vol. 327, no. 5973, pp. 1603–1607, 2010.

[135] X. Huang *et al.*, "Epidermal radio frequency electronics for wireless power transfer," *Microsystems Nanoeng.*, vol. 2, no. June, pp. 1–9, 2016.

[136] H.-J. Kim, C. Yu, K. Sim, Z. Rao, A. Thukral, and H. Shim, "Fully rubbery integrated electronics from high effective mobility intrinsically stretchable semiconductors," *Sci. Adv.*, vol. 5, no. 2, p. eaav5749, 2019.

[137] J. H. Cho *et al.*, "Printable ion-gel gate dielectrics for low-voltage polymer thin-film transistors on plastic," *Nat. Mater.*, vol. 7, no. 11, pp. 900–906, 2008.

[138] J. Veres, S. D. Ogier, S. W. Leeming, D. C. Cupertino, and S. M. Khaffaf, "Low-k insulators as the choice of dielectrics in organic field-effect transistors," *Adv. Funct. Mater.*, vol. 13, no. 3, pp. 199–204, 2003.

[139] L. Feng *et al.*, "Unencapsulated Air-stable Organic Field Effect Transistor by All Solution Processes for Low Power Vapor Sensing," *Sci. Rep.*, vol. 6, no. October 2015, p. 20671, 2016.

[140] H. Sirringhaus, "Reliability of organic field-effect transistors," *Adv. Mater.*, vol. 21, no. 38–39, pp. 3859–3873, 2009.

[141] W. H. Lee, H. H. Choi, D. H. Kim, and K. Cho, "Microstructure Dependent Bias Stability of Organic Transistors," *Adv. Mater.*, vol. 26, no. 11, pp. 1660–1680, 2014.

[142] S. G. J. Mathijssen *et al.*, "Dynamics of threshold voltage shifts in organic and amorphous silicon field-effect transistors," *Adv. Mater.*, vol. 19, no. 19, pp. 2785–2789, 2007.

[143] E. Sowade *et al.*, "Up-scaling of the manufacturing of all-inkjet-printed organic thin-film transistors: Device performance and manufacturing yield of transistor arrays," *Org. Electron.*, vol. 30, pp. 237–246, 2016.

[144] Y. H. Kim, B. Yoo, J. E. Anthony, and S. K. Park, "Controlled deposition of a high-performance small-molecule organic single-crystal transistor array by direct ink-jet printing," *Adv. Mater.*, vol. 24, no. 4, pp. 497–502, 2012.

[145] B. K. C. Kjellander, W. T. T. T. Smaal, J. E. Anthony, and G. H. Gelinck, "Inkjet printing of TIPS-PEN on soluble polymer insulating films: A route to high-performance thin-film transistors," *Adv. Mater.*, vol. 22, no. 41, pp. 4612–4616, 2010.

[146] J. A. Lim, W. H. Lee, D. Kwak, and K. Cho, "Evaporation-Induced Self-Organization of Inkjet-Printed Organic Semiconductors on Surface-Modified Dielectrics for High-Performance Organic Transistors," *Langmuir*, vol. 25, no. 9, pp. 5404–5410, 2009.

[147] M. R. Niazi *et al.*, "Contact-induced nucleation in high-performance bottom-contact organic thin film transistors manufactured by large-area compatible solution processing," *Adv. Funct. Mater.*, vol. 26, no. 14, pp. 2371–2378, 2016.

[148] J. E. Anthony, "Functionalized acenes and heteroacenes for organic electronics," *Chem. Rev.*, vol. 106, no. 12, pp. 5028–5048, 2006.

[149] J. A. Lim, H. S. Lee, W. H. Lee, and K. Cho, "Control of the morphology and structural development of solution-processed functionalized acenes for high-performance organic transistors," *Adv. Funct. Mater.*, vol. 19, no. 10, pp. 1515–1525, 2009.

[150] Y. Diao *et al.*, "Solution coating of large-area organic semiconductor thin films with aligned single-crystalline domains," *Nat. Mater.*, vol. 12, no. 7, pp. 665–671, 2013.

[151] L. Ding, J. Zhao, Y. Huang, W. Tang, S. Chen, and X. Guo, "Flexible-Blade Coating of Small Molecule Organic Semiconductor for Low Voltage Organic Field Effect Transistor," *IEEE Electron Device Lett.*, vol. 38, no. 3, pp. 338–340, 2017.

[152] F. Paulus *et al.*, "Side-group engineering : The in fl uence of norbornadienyl substituents on the properties of ethynylated pentacene and tetraazapentacene," *Org. Electron.*, vol. 33, pp. 102–109, 2016.

[153] S. Chung, S. O. Kim, S. K. Kwon, C. Lee, and Y. Hong, "All-inkjet-printed organic thin-film transistor inverter on flexible plastic substrate," *IEEE Electron Device Lett.*, vol. 32, no. 8, pp. 1134–1136, 2011.

[154] S. Y. Cho, J. M. Ko, J. Lim, J. Y. Lee, and C. Lee, "Inkjet-printed organic thin film transistors based on TIPS pentacene with insulating polymers," *J. Mater. Chem. C*, vol. 1, no. 5, pp. 914–923, 2013.

[155] X. Wang *et al.*, "Process optimization for inkjet printing of triisopropylsilylethynyl pentacene with single-solvent solutions," *Thin Solid Films*, vol. 578, pp. 11–19, 2015.

[156] M. W. Lee, G. S. Ryu, Y. U. Lee, C. Pearson, M. C. Petty, and C. K. Song, "Control of droplet morphology for inkjet-printed TIPS-pentacene transistors," *Microelectron. Eng.*, vol. 95, pp. 1–4, 2012.

[157] M. Medina-Sánchez, C. Martínez-Domingo, E. Ramon, and A. Merkoçi, "An inkjet-printed field-effect transistor for label-free biosensing," *Adv. Funct. Mater.*, vol. 24, no. 40, pp. 6291–6302, 2014.

[158] D. T. James, J. M. Frost, J. Wade, J. Nelson, J. Kim, and J. E. T. Al, "Controlling Microstructure of Pentacene Derivatives by Solution Processing : Impact of Structural Anisotropy on Optoelectronic Properties," *ACS Nano*, vol. 7, no. 9, pp. 7983–7991, 2013.

[159] H. Minemawari *et al.*, "Inkjet printing of single-crystal films," *Nature*, vol. 475, no. 7356, pp. 364–367, 2011.

[160] K. Nakayama *et al.*, "Patternable solution-crystallized organic transistors with high charge carrier mobility," *Adv. Mater.*, vol. 23, no. 14, pp. 1626–1629, 2011.

[161] J. Tsurumi *et al.*, "Coexistence of ultra-long spin relaxation time and coherent charge transport in organic single-crystal semiconductors," *Nat. Phys.*, vol. 13, no. 10, pp. 994–998, 2017.

[162] H. Y. Tseng and V. Subramanian, "All inkjet-printed, fully self-aligned transistors for low-cost circuit applications," *Org. Electron.*, vol. 12, no. 2, pp. 249–256, 2011.

[163] M. Noda *et al.*, "An OTFT-driven rollable OLED display," *J. Soc. Inf. Disp.*, vol. 19, no. 4, pp. 316–322, 2011.

[164] E. Gili, M. Caironi, and H. Sirringhaus, "Organic integrated complementary inverters with ink-jet printed source/drain electrodes and sub-micron channels," *Appl. Phys. Lett.*, vol. 100, no. 12, pp. 1–5, 2012.

[165] T. Umeda, D. Kumaki, and S. Tokito, "High air stability of threshold voltage on gate bias stress in pentacene TFTs with a hydroxyl-free and amorphous fluoropolymer as gate insulators," *Org. Electron.*, vol. 9, no. 4, pp. 545–549, 2008.

[166] C. Jiang, H. Ma, and Arokia Nathan, "Stability Analysis of All-Inkjet-Printed Organic Thin-Film Transistors," *MRS Adv.*, vol. 357, no. May, pp. 1–8, 2017.

[167] X. Ren *et al.*, "A Low-Operating-Power and Flexible Active-Matrix Organic-Transistor Temperature-Sensor Array," *Adv. Mater.*, pp. 4832–4838, 2016.

[168] T. Sekitani *et al.*, "Ultraflexible organic amplifier with biocompatible gel electrodes," *Nat. Commun.*, vol. 7, pp. 1–11, 2016.

[169] D. Mantini, M. G. Perrucci, C. Del Gratta, G. L. Romani, and M. Corbetta, "Electrophysiological signatures of resting state networks in the human brain.," *Proc. Natl. Acad. Sci.*, vol. 104, no. 32, pp. 13170–5, 2007.

[170] H. Klauk, U. Zschieschang, J. Pflaum, and M. Halik, "Ultralow-power organic complementary circuits.," *Nature*, vol. 445, no. 7129, pp. 745–8, 2007.

[171] J. Li, Z. Sun, and F. Yan, "Solution processable low-voltage organic thin film transistors with high-k relaxor ferroelectric polymer as gate insulator," *Adv. Mater.*, vol. 24, no. 1, pp. 88–93, 2012.

[172] W. Tang, J. Li, J. Zhao, W. Zhang, F. Yan, and X. Guo, "High-Performance Solution-Processed Low-Voltage Polymer Thin-Film Transistors With Low-k/High-k Bilayer Gate Dielectric," *IEEE Electron Device Lett.*, vol. 36, no. 9, pp. 950–952, 2015.

[173] W. Tang *et al.*, "Bias stress stability improvement in solution-processed low-voltage organic field-effect transistors using relaxor ferroelectric polymer gate dielectric," *IEEE Electron Device Lett.*, vol. 38, no. 6, pp. 748–751, 2017.

[174] S. D. Brotherton, *Introduction to thin film transistors: Physics and technology of TFTs*. Switzerland: Springer International Publishing, 2013.

[175] C. Wang, H. Dong, W. Hu, Y. Liu, and D. Zhu, "Semiconducting π-Conjugated Systems in Field-Effect Transistors: A Material Odyssey of Organic Electronics," *Chem. Rev.*, vol. 112, pp. 2208–2267, 2012.

[176] L. Feng, W. Tang, X. Xu, Q. Cui, and X. Guo, "Ultralow-voltage solution-processed organic transistors with small gate dielectric capacitance," *IEEE Electron Device Lett.*, vol. 34, no. 1, pp. 129–131, 2013.

[177] L. Feng, W. Tang, J. Zhao, Q. Cui, C. Jiang, and X. Guo, "All-solution-processed low-voltage organic thin-film transistor inverter on plastic substrate," *IEEE Trans. Electron Devices*, vol. 61, no. 4, pp. 1175–1180, 2014.

[178] W. Tang *et al.*, "Controlling the surface

wettability of the polymer dielectric for improved resolution of inkjet-printed electrodes and patterned channel regions in low-voltage solution-processed organic thin film transistors," *J. Mater. Chem. C*, vol. 2, no. 28, p. 5553, 2014.

[179] K. Takimiya, H. Ebata, K. Sakamoto, T. Izawa, T. Otsubo, and Y. Kunugi, "2,7-Diphenyl[1]benzothieno[3,2-b]benzothiophene, a new organic semiconductor for air-stable organic field-effect transistors with mobilities up to 2.0 cm2 V-1 s-1," *J. Am. Chem. Soc.*, vol. 128, no. 39, pp. 12604–12605, 2006.

[180] T. Yamamoto and K. Takimiya, "Facile synthesis of highly π-extended heteroarenes, dinaphtho[2,3-b: 2′,3′-f]chalcogenopheno[3,2-b]chalcogenophenes, and their application to field-effect transistors," *J. Am. Chem. Soc.*, vol. 129, no. 8, pp. 2224–2225, 2007.

[181] P. Gao *et al.*, "Dithieno[2,3-d;2′3′-d′]benzo[1,2-b;4,5-b′] dithiophene (DTBDT) as semiconductor for high-performance, solution-processed organic field-effect transistors," *Adv. Mater.*, vol. 21, no. 2, pp. 213–216, 2009.

[182] H. Iino, T. Usui, and J. Hanna, "Liquid crystals for organic thin-film transistors," *Nat. Commun.*, vol. 6, pp. 1–8, 2015.

[183] M. Kunii, H. Iino, and J. Hanna, "Organic Field-Effect Transistor Fabricated Using Highly Ordered Liquid Crystal With Low- k Gate Dielectric," *IEEE Electron Device Lett.*, vol. 37, no. 4, pp. 486–488, 2016.

[184] X. Cheng, S. Lee, and A. Nathan, "Deep Subthreshold TFT Operation and Design Window for Analog Gain Stages," *IEEE J. Electron Devices Soc.*, vol. 6, no. 1, pp. 195–200, 2018.

[185] X. Cheng, S. Lee, G. Yao, and A. Nathan, "TFT Compact Modeling," *J. Disp. Technol.*, vol. 12, no. 9, pp. 898–906, 2016.

[186] F. N. Hooge, T. G. M. Kleinpenning, and L. K. J. Vandamme, "Experimental studies on 1/f noise," *Reports Prog. Phys.*, vol. 44, no. 5, pp. 479–532, 1981.

[187] D. V. Lang, X. Chi, T. Siegrist, A. M. Sergent, and A. P. Ramirez, "Amorphouslike density of gap states in single-crystal pentacene," *Phys. Rev. Lett.*, vol. 93, no. 8, pp. 8–11, 2004.

[188] G. Fortunato, D. B. Meakin, P. Migliorato, and P. G. Le Comber, "Field-effect analysis for the determination of gap-state density and fermi-level temperature dependence in poly crystalline silicon," *Philos. Mag. B Phys. Condens. Matter; Stat. Mech. Electron. Opt. Magn. Prop.*, vol. 57, no. 5, pp. 573–586, 1988.

[189] W. L. Kalb and B. Batlogg, "Calculating the trap density of states in organic field-effect transistors from experiment: A comparison of different methods," *Phys. Rev. B*, vol. 81, no. 3, p. 035327, 2010.

[190] W. L. Kalb, S. Haas, C. Krellner, T. Mathis, and B. Batlogg, "Trap density of states in small-molecule organic semiconductors: A quantitative comparison of thin-film transistors with single crystals," *Phys. Rev. B*, vol. 81, p. 155315, 2010.

[191] J. Puigdollers, a. Marsal, S. Cheylan, C. Voz, and R. Alcubilla, "Density-of-states in pentacene from the electrical characteristics of thin-film transistors," *Org. Electron. physics, Mater. Appl.*, vol. 11, no. 8, pp. 1333–1337, 2010.

[192] K. Weber, M. Grünewald, W. Fuhs, and P. Thomas, "Field Effect in a-Si:H Films," *Phys. Status Solidi*, vol. 133, pp. 133–142, 1982.

[193] J. Zhao *et al.*, "Universal Compact Model for Thin-Film Transistors and Circuit Simulation for Low-Cost Flexible Large Area Electronics," *IEEE Trans. Electron Devices*, vol. 64, no. 5, pp. 2030–2037, 2017.

[194] H. Aoki, "Dynamic characterization of a-Si TFT-LCD pixels," *IEEE Trans. Electron Devices*, vol. 43, no. 1, pp. 31–39, 1996.

[195] K. S. Karim, P. Servati, N. Mohan, A. Nathan, and J. A. Rowlands, "VHDL-AMS modeling and simulation of a passive pixel sensor in a-Si:H technology for medical imaging," in *ISCAS 2001. The 2001 IEEE International Symposium on Circuits and Systems (Cat. No.01CH37196)*, vol. 5, pp. 479–482.

[196] M. Fadlallah, W. Benzarti, G. Billiot, W. Eccleston, and D. Barclay, "Modeling and characterization of organic thin film transistors for circuit design," *J. Appl. Phys.*, vol. 99, no. 10, p. 104504, 2006.

[197] A. Valletta *et al.*, "A compact Spice model for organic TFTs and applications to logic circuit design," in *2015 IEEE 15th International Conference on Nanotechnology (IEEE-NANO)*, 2015, pp. 1434–1437.

[198] H.-H. Hsieh, T. Kamiya, K. Nomura, H. Hosono, and C.-C. Wu, "Modeling of amorphous InGaZnO[sub 4] thin film transistors and their subgap density of states," *Appl. Phys. Lett.*, vol. 92, no. 13, p. 133503, 2008.

[199] S. Lee *et al.*, "Trap-limited and percolation conduction mechanisms in amorphous oxide semiconductor thin film transistors," *Appl. Phys. Lett.*, vol. 98, 2011.

[200] S. Lee, S. Jeon, and A. Nathan, "Modeling Sub-Threshold Current–Voltage Characteristics in Thin Film Transistors," *J. Disp. Technol.*, vol. 9, no. 11, pp. 883–889, Nov. 2013.

[201] S. Lee and A. Nathan, "Localized tail state distribution in amorphous oxide transistors deduced from low temperature measurements," *Appl. Phys. Lett.*, vol. 101, no. 11, p. 113502, 2012.

[202] S. Lee, D. Striakhilev, S. Jeon, and A. Nathan, "Unified Analytic Model for Current–Voltage Behavior in Amorphous Oxide Semiconductor TFTs," *IEEE Electron Device Lett.*, vol. 35, no. 1, pp. 84–86, Jan. 2014.

[203] Z. Zong, L. Li, J. Jang, N. Lu, and M. Liu, "Analytical surface-potential compact model for amorphous-IGZO thin-film transistors," *J. Appl. Phys.*, vol. 117, no. 21, p. 215705, 2015.

[204] C. Perumal *et al.*, "A compact a-IGZO TFT model based on MOSFET SPICE Level=3 template for Analog/RF circuit designs," *IEEE Electron Device Lett.*, vol. 34, no. 11, pp. 1391–1393, 2013.

[205] K. Khakzar and E. H. Lueder, "Modeling of amorphous-silicon thin-film transistors for circuit simulations with SPICE," *IEEE Trans. Electron Devices*, vol. 39, no. 6, pp. 1428–1434, Jun. 1992.

[206] L. Resendiz, B. Iniguez, a. Estrada, and a. Cerdeira, "Modification of amorphous level 15 AIM SPICE model to include new subthreshold model," *2004 24th Int. Conf. Microelectron. (IEEE Cat. No.04TH8716)*, vol. 1, pp. 16–19, 2004.

[207] T. Leroux, "Static and dynamic analysis of amorphous-silicon field-effect transistors," *Solid. State. Electron.*, vol. 29, no. 1, pp. 47–58, Jan. 1986.

[208] M. S. Shur, "SPICE Models for Amorphous Silicon and Polysilicon Thin Film Transistors," *J. Electrochem. Soc.*, vol. 144, no. 8, p. 2833, 1997.

[209] M. Shur, M. Hack, and J. G. Shaw, "A new analytic model for amorphous silicon thin-film transistors," *J. Appl. Phys.*, vol. 66, no. 7, p. 3371, 1989.

[210] G. Horowitz and P. Delannoy, "An analytical model for organic-based thin-film transistors," *J. Appl. Phys.*, vol. 70, no. 1, p. 469, 1991.

[211] M. C. J. M. Vissenberg and M. Matters, "Theory of the field-effect mobility in amorphous organic transistors," vol. 57, no. 20, p. 13, 1998.

[212] M. Estrada *et al.*, "Accurate modeling and parameter extraction method for organic TFTs," *Solid. State. Electron.*, vol. 49, no. 6, pp. 1009–1016, Jun. 2005.

[213] J. Fan, J. Zhao, and X. Guo, "DC Compact Model for Subthreshold Operated Organic Field-Effect Transistors," *IEEE Electron Device Lett.*, vol. 39, no. 8, pp. 1191–1194, 2018.

[214] "IEEE Recommended Practices #P1485 on: Test Procedures for Micro-electronic MOSFET Circuit Simulator Model Validation," 1997. .

[215] X. Cheng, S. Lee, and A. Nathan, "TFT Small Signal Model and Analysis," *IEEE Electron Device Lett.*, vol. 37, no. 7, pp. 890–893, 2016.

[216] M. Elsobky *et al.*, "A digital library for a flexible low-voltage organic thin-film transistor technology," *Org. Electron. physics, Mater. Appl.*, vol. 50, pp. 491–498, 2017.

[217] Y. Takeda *et al.*, "Fabrication of Ultra-Thin printed organic TFT CMOS logic circuits optimized for low-voltage wearable sensor applications," *Sci. Rep.*, vol. 6, no. April, pp. 1–9, 2016.

[218] M. Choi, Y. J. Park, B. K. Sharma, S.-R. Bae, S. Y. Kim, and J.-H. Ahn, "Flexible active-matrix organic light-emitting diode display enabled by MoS2 thin-film transistor," *Sci. Adv.*, vol. 4, no. 4, p. eaas8721, 2018.

[219] J. Park *et al.*, "Research on flexible display at Ulsan National Institute of Science and Technology," *npj Flex. Electron.*, vol. 1, no. 1, pp. 1–12, 2017.

[220] S. Harada *et al.*, "Printed multifunctional flexible device with an integrated motion

sensor for health care monitoring," *Sci. Adv.*, vol. 2, no. 11, p. e1601473, 2016.

[221] D. Jang, D. Kim, and J. Moon, "Influence of fluid physical properties on ink-jet printability," *Langmuir*, vol. 25, no. 5, pp. 2629–2635, 2009.

ABOUT THE AUTHORS

Chen Jiang (S'17–M'19) received the B.S. degree in engineering from Shanghai Jiao Tong University, China, in 2014, and his Ph.D. degree in engineering at the University of Cambridge, UK, in 2019.

He is currently a Junior Research Fellow with the University of Cambridge. In his Ph.D. study, he worked on exploring novel electronic devices for low-power, low-cost electronics, encompassing device fabrication, and device physics and modeling. His research interests include novel electronic device architectures, printable large-area electronics, and low-power circuits for wearable/implantable sensor interface systems. He was a recipient of the Cambridge International Scholarship Scheme and the China Scholarship Council Scholarship, and was also the winner of the Cambridge Society for the Application of Research Award 2018.

Dr Jiang was a receipt of the IEEE Electron Devices Society PhD Student Fellowship 2018.

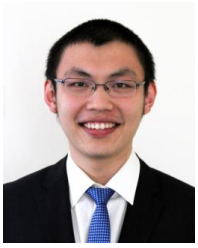

Xiang Cheng (S'15-M'18) received his bachelor degree in electronic engineering from Shanghai Jiao Tong University in 2013, and his PhD at the University of Cambridge in 2017. Following one-year post-doctoral period at the University of Cambridge, he then joined Cambridge Touch Technology LTD as a system architect engineer.

During his time at SJTU and subsequently at Cambridge, he worked on AMOLED pixel circuit design and device simulation seeking compensation solutions and new circuit architectures. His research interests span a broad range of area including fundamental device physics and system integration of emerging touch technology.

Arokia Nathan (S'84–M'87–SM'99–F'10) received the Ph.D. degree in electrical engineering from the University of Alberta.

Following post-doctoral years at LSI Logic Corp., USA, and ETH Zurich, Switzerland, he joined the University of Waterloo, Canada, where he held the DALSA/NSERC Industrial Research Chair in sensor technology and subsequently the Canada Research Chair in nano-scale flexible circuits. He was a recipient of the 2001 NSERC E.W.R. Steacie Fellowship. In 2006, he moved to the U.K. to take up the Sumitomo Chair of Nanotechnology at the London Centre for Nanotechnology, University College London, and subsequently held the Chair of Photonic Systems and Displays in the Department of Engineering, Cambridge University, where he led a multi-disciplinary research group working on the heterogeneous integration of materials and processes, sensors, energy harvesting and storage devices pertinent to wearable technologies. He is currently the Chief Technical Officer of Cambridge Touch Technologies, a company spun out of the University developing advanced interactive technologies. He received the Royal Society Wolfson Research Merit Award and recently the BOE Distinguished Contribution Award for TFT Compact Modeling and Circuit Design. He has held Visiting Professor appointments at the Physical Electronics Laboratory, ETH Zürich and the Engineering Department, Cambridge University, U.K. He has published over 600 papers in the field of sensor technology, CAD, thin film transistor electronics, and is a co-author of four books. He has over 70 patents filed/awarded and has founded/co-founded four spin-off companies. He serves on technical committees and editorial boards in various capacities.

Dr. Nathan is a Chartered Engineer (U.K.), Fellow of the Institution of Engineering and Technology (UK), Fellow of IEEE (USA), and an IEEE/EDS Distinguished Lecture.